Synthesis and Characterization of Zinc and Nickel-doped Cobalt Oxide Nanoparticles and their Biological Applications

Submitted by

Saima Faiz

619-FOS/MSBT/F23

Department of Biological Sciences

Faculty of Sciences

International Islamic University, Islamabad

(2025)

Synthesis and Characterization of Zinc and Nickel-doped Cobalt Oxide Nanoparticles and their Biological Applications

Submitted by

Saima Faiz

619-FOS/MSBT/F23

Supervisor

Dr. Shaheen Shahzad

Assistant Professor

Co-supervisor

Dr. Rehana Riaz

Assistant Professor

Department of Biological Sciences

Faculty of Sciences

International Islamic University, Islamabad

(2025)

Department of Biological Sciences

International Islamic University Islamabad

Dated _____

APPROVAL CERTIFICATE

It is to certify that this project meets the entire requirements and warrants its acceptance by the Department of Biotechnology, International Islamic University, Islamabad for the degree of MS Biotechnology for Saima Faiz (619-FBAS/MSBT/F23).

COMMITTEE

Supervisor

Dr. Shaheen Shahzad

Department of Biological Sciences, IIUI _____

Co-supervisor

Dr. Rehana Riaz

Department of Physics, IIUI _____

Internal Examiner

Dr.

Department of Biological Sciences, IIUI

International Islamic University, Islamabad _____

Chair person

Prof. Dr. Asma Gul

Department of Biological Sciences, IIUI

International Islamic University, Islamabad _____

Dean, FOS

Prof. Dr Mushtaq Ahmad

International Islamic University, Islamabad _____

DEDICATION

This effort is dedicated to

My Family

Declaration

I hereby declare that this thesis "**Synthesis and characterization of Zinc and Nickel-doped Cobalt oxide Nanoparticles"** as a whole nor as a part has been copied out from any source. It is further declared that I have done this research with the accompanied report entirely based on my efforts, under the proficient guidance of Dr. Shaheen Shahzad (Supervisor). I also declare that the work presented in this thesis has not been submitted in support of any other application or degree or qualification in any other University or Institute.

Saima Faiz

619/FBAS/MSBT/F23

Saima.msbt619@student.iiu.edu.pk

TABLE OF CONTENTS

ACKNOWLEDGEMENTS

My first and foremost obligation is to thank the Almighty Allah for giving me enough strength and courage to complete this dissertation

This research was made possible through the unwavering support and guidance of my supervisor, ***Dr. Shaheen Shahzad****. I feel truly blessed to have her mentorship throughout the entire period of this study. I am deeply indebted to my co-supervisor,* ***Dr. Rehana Riaz*** *whose kindness, expertise, and inspiring personality have been unmatched. I am incredibly fortunate to have such a sincere and dedicated supervisor and teacher in my life.*

I would like to express my heartfelt gratitude to the International Islamic University and ***Prof. Dr. Asif Mir,*** *Chairperson of the Department of Biological Sciences, for their timely facilitation, which expedited the entire course of this work. My sincere thanks also go to* ***Dr. Ifrah****, for her caring attitude, guidance, and helpful discussions. I am also profoundly grateful to CAEPE and all my fellows of Genomics Research Lab for their invaluable assistance in my project completion. I extend my warmest thanks to* ***Dr. Robina Khan Niazi,*** *Lab Manager, and* ***Ms. Rukhsana****, Lab Assistant, for their overwhelming support in providing an uninterrupted working environment and ensuring that all prerequisites for the experimental investigations were met.*

A very heartiest thanks to my family. Words cannot express how grateful I am to my ***father, mother****,* ***sister and brother, Adnan*** *for all the prayers and support. I would like to say special thanks to my husband for his unwavering support. Thank you for always being so encouraging and supportive in every matter of my life.*

Last but not least, I'd like to express my heartfelt gratitude and love to my parents and son, ***Arham Waheed*** *for staying at home without me and understanding that mama needs to attend university to completer her*

MS.SAIMA FAIZ

LIST OF ABBREVIATIONS

Abbreviation	**Definition**
NPs	Nanoparticles
%	Percentage
°C	Degree Calcius
µg/µL	Microgram per microliter
µL	Microliter
µg	Microgram
mL	Milliliter
mm	Millimeter
mg/L	Milligram per liter
nm	Nanometer
cm^{-1}	Per centimeter
S.D	Standard Deviation
S.E	Standard error
≥	Greater and equal
$C_4H_6CoO_4$	Cobalt Acetate
Co_3O_4	Cobalt oxide

$O_2^{\bullet -}$	Superoxide Radical Anions
XRD	X ray Diffraction
SEM	Scanning Electron Microscopy
FTIR	Fourier Transform Infrared Spectroscopy
DNA	Deoxyribonucleic Acid
UV-VIS	Ultraviolet Visible Spectroscopy
ZnO	Zinc oxide
NiO	Nickel oxide
ROS	Reactive oxygen species
MONPs	Metal oxide nanoparticles
U87	Human brain cancer (glioblastoma) cell line
DMSO	Dimethyl Sulfoxide
IC_{50}	Inhibitory concentration at 50%
ISO	International Organization for Standardization
MTT	3-(4,5-dimethylthiazol-2-yl)-2,5-diphenyltetrazolium bromide.
OER	Oxygen Evolution Reaction
Zn Co_3O_4	Zinc-doped Cobalt Oxide

θ	Angle
Ni Co_3O_4	Nickel-doped Cobalt oxide
NB	Nutrient broth
eV	Electron volts
E_g	Band gap energy
FWHM	Full width at half maximum
°	Degree
JCPDS	Joint Committee on Powder Diffraction Standards

LIST OF FIGURES

LIST OF TABLES

ABSTRACT

Antimicrobial resistance and oncological disorders represent predominant challenges within the domain of medical sciences. The present research focuses on the development of Zinc and Nickel-doped cobalt oxide nanostructures, using a Co-precipitation approach and their evaluation for biomedical applications. The properties of these nanostructures concerning structure, morphology, functional groups, and optical characteristics were examined through X-ray diffraction (XRD), scanning electron microscopy (SEM), Fourier-transform infrared spectroscopy (FTIR) and UV-Vis spectroscopy. X-ray diffraction analysis elucidated the crystalline characteristics of the doped nanoparticles. SEM examination revealed that the synthesized nanoparticles exhibited a spherical morphology.The antibacterial efficacy was evaluated against both Gram-positive (*Staphylococcus*) and Gram-negative (*Klebsiella, Salmonella, and Acinetobacter*) bacterial strains by disk diffusion method. Notably, the Ni-doped Co_3O_4 nanoparticles demonstrated their peak mean activity against *Klebsiella pneumoniae* (13 ± 0.5 mm), whereas the Zn-doped Co_3O_4 nanoparticles exhibited the highest mean antibacterial efficacy against *Salmonella enteritidis* (22 ± 1 mm). Furthermore, the MTT assay was employed to evaluate the cytotoxic effects of cobalt oxide nanoparticles doped with Zinc and Nickel on the brain cancer cell line U87, revealing a dose-dependent inhibition of cell proliferation. Exposures exceeding 500 µg/µL resulted in complete destruction of viable cells in Zn-doped Co_3O_4, indicating pronounced cytotoxicity at elevated concentrations. Conversely, even at relatively low concentrations, Ni-doped Cobalt oxide displayed significant cytotoxic effects. Zinc-doped Cobalt oxide. Cobalt oxide nanoparticles that have been doped with Zinc displayed enhanced anticancer and antibacterial efficacy, indicating a greater cytotoxic impact on neoplastic cells and a more robust inhibition of bacterial growth in comparison to both undoped Cobalt oxide and Cobalt oxide doped with Nickel.

1.INTRODUCTION

The use of nanoscale methods and materials in biological systems is known as nano biotechnology. It entails studying and modifying biological processes at the molecular level by the use of nanomaterials, including nanoparticles, nanotubes, and nanosensors (Iqbal *et al.,* 2024). Nanobiotechnology provides new pathways to improve efficiencies in today's technology and demonstrates new approaches for addressing global issues, such as food security, disease prevention, and environmental degradation. Particles with a diameter of approximately 1 to 100 nanometers are identified as nanoparticles. Because of their unique dimensions, nanoparticles exhibit different physical and chemical properties than larger particles of the same materials. The properties of nanoscale materials exploit the unique aspects of such small biologically-relevant materials, including the high surface area, reactivity, and small dimensions, to improve drug delivery, disease diagnosis, and therapeutic delivery (Shahcheraghi *et al.,* 2022). Nanoparticles can be classified based on a criteria, such as composition, structure, and application. Nanoparticles have been heavily researched and used in biomedicine for the past 50 years, partly because of their non-invasiveness, simplicity of temporal (time) and spatial (space) manipulation, and large biocompatibility and biodistribution. Understanding Nano-bio interactions is necessary to ensure that nanomaterials are safe and effective for use. Almost every property of nanoparticles will direct how they pass through some biological systems, interact with cells in those biological systems, and spread (deposition and distribution) in whole organisms. The nanoparticle-cell interactions are paramount, and in their study, researchers often focus on how surface charge, size, shape, and chemical activity affect biomolecular signaling (Bukhari *et al*., 2021).

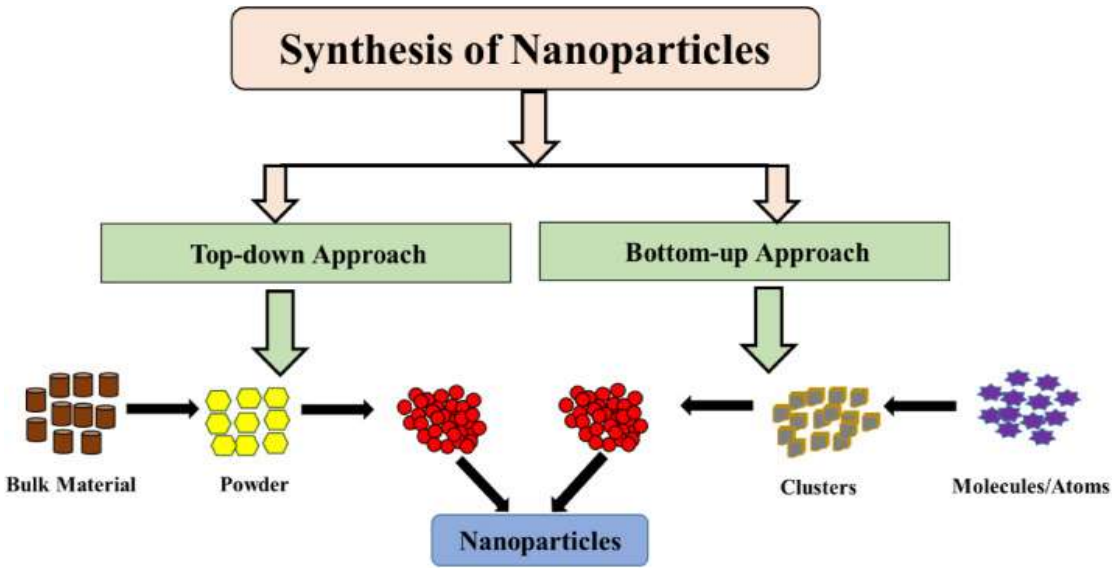

Figure 1.1 Synthetic techniques for metal and metal oxide nanoparticles: top-down and bottom-up (Kumari *et al.*, 2023)

Cobalt oxide (Co_3O_4) nanoparticles are a valuable research topic given their unique properties and versatility. Cobalt oxide nanoparticles appear as dark brown or black powder, and exhibit a spinel crystal structure, (Shete *et al.*, 2022). They have biological interactions that can have cytotoxic effects in cancer cells and inhibit bacterial growth (Waris, 2021). ZnO nanoparticles have the potential for biocompatibility, low toxicity and antimicrobial activity (Alhujaily, 2022). They are capable of producing reactive oxygen species (ROS) that can have damaging effects on bacteria and lead to apoptosis in cancer cells. NiO nanoparticles possessed antifungal, antibacterial, and catalytic properties (Khalil, 2017).

Doping is the addition of a few foreign atoms to lattice structure of a material for property modification (Selvam, 2024). Doping of particles made from metal oxide nanoparticles to potentially enhance the activity of the nanoparticles against the microbes or improved the anticancer ability of the nanoparticles against cancers and enhance the nanoparticles' surface area and reactivity. As an example, when ZnO is doped with cobalt, the Co doped ZnO nanoparticles improved antibacterial, anticancer, and ROS generation activity (Shenoy, 2022). The combination of cobalt oxide with Zinc and Nickel, could potentially exploit the synergistic effect on antibacterial and

anticancer, through improved ROS generation (Khalid, 2021) improved antimicrobial and anticancer activity against brain cancer. (Almoneef, 2024). Selected targeting should kill cancer cells with little or no harm to normal cells (Faisal *et al*., 2020). The main mechanisms include activating the apoptotic caspase pathways, particularly caspase-3 and producing DNA damage primarily through the formation of reactive oxygen species (ROS) ultimately leading to oxidative stress and cellular destruction (Samri *et al.*, 2021).

Various methods are used for Zinc and Nickel-doped cobalt oxide nanoparticles. Hydrothermal, sol gel method and co-precipitation method. These synthesis methods not only produce nanoparticles but also maximize their antibacterial effectiveness by ensuring that the Zinc and Nickel are uniformly distributed within the cobalt oxide framework, a critical factor in optimizing their physical and chemical properties (Naseri *et al.*, 2016). Because of its similar composition and ease of usage, the co-precipitation method is employed in this case.

Characterization of nanoparticles is important for revealing their physicochemical properties, which ultimately determine their biological activities and possible uses. Some of the most common techniques for characterization include X-ray diffraction (XRD), scanning electron microscopy (SEM), Fourier-transform infrared spectroscopy (FTIR), and UV-Vis spectroscopy. Each technique can provide information on the crystal structure, morphology, surface chemistry, and optical features of the nanoparticles (Almoneef *et al.*, 2024). Zinc and Nickel-doped Cobalt oxide nanoparticles exhibit improved biological and catalytic properties with a variety of applications. These nanoparticles represent enhanced antimicrobial activity, which many researchers have reported (Al Enazi *et al.*, 2023). The anticancer ability of these effective agents is enhanced by doping, as they exhibit increased cytotoxicity and ROS production and have been utilized as promising agents for cancer therapy (Anjum *et al.*, 2022). These nanoparticles possess numerous advantages in an environmental and catalytic sense, as with improved bioremediation of organic pollutants and even offer enzyme-like activity to help improve the degradation of organic pollutants in wastewater treatment (Li *et al.*, 2022).

Aim and objectives

The primary aim of the research is to synthesize and characterize Zinc and Nickle doped Cobalt Oxide nanoparticles and check their antibacterial and anticancer activities with following objectives:

i. To synthesize Zinc and Nickel-doped cobalt oxide using co-precipitation method
ii. To characterize the nanostructures using different techniques
iii. To evaluate their antibacterial activity against pathogenic bacteria
iv. To investigate their anticancer potential on brain cancer cell line.

2. LITERATURE REVIEW

Materials and systems at the nanoscale, usually 1 to 100 nanometers, are being investigated in nanoscience. Materials have intrinsic physical, chemical, and biological characteristics that are absent from their macroscopic counterparts, making it a crucial scale. Numerous industries, including materials research and biomedical applications, are being revolutionized by the new high surface area-to-volume ratios and quantum phenomena that are specific of the scale (Naik & Mallikarjun, 2023).

2.1 Nanoparticles

Nanoparticles are defined as particles with dimensions ranging from 1 to 100 nanometers (nm) in diameter. Their unique size allows them to exhibit distinct physical and chemical properties compared to larger particles of the same material. This size range is critical because it is where many novel phenomena occur, enabling a variety of applications across multiple fields, including medicine, environmental science, and materials engineering (Dobson *et al*., 2024).

2.1.1 Size and Structure: All three external dimensions of a nanoparticle should be smaller than 100 nm, according to the International Organization for Standardization (ISO). In order to be categorized as nanoparticles, the European Union's definition highlights that at least 50% of the particles must fall within this size range.

2.1.2 Unique Properties: Nanoparticles often possess enhanced properties due to their high ratio of surface area to volume. This can lead to increased reactivity, altered optical characteristics, and improved electrical properties compared to their bulk counterparts (Altamar, 2023).

2.2 Nano biotechnology

Nano biotechnology is an emerging branch of science which uses nanotechnology in the biological field. It uses biological materials which are in the Nano size range. It has applications in various aspects of life as in medical, agricultural, industrial, environment and biological sciences. It leads to significant improvement in various techniques like drug delivery, food processing, tissue engineering and enzymatic

processes (Hijam & Laishram, 2020). Nanoparticles are complex itself and composed of following layers

a) The surface layer, which can be coated with metal ions, polymers, surfactants, and a variety of tiny molecules.
b) The shell layer, which is entirely made of chemically distinct material from the core.
c) The core, which is essentially the nanoparticles' central region (Shin *et al.*, 2016).

2.3 Classification of Nanoparticles

As shown in figure 2.1, nanoparticles can be categorized according to a number of factors, including their composition, structure, and intended use.

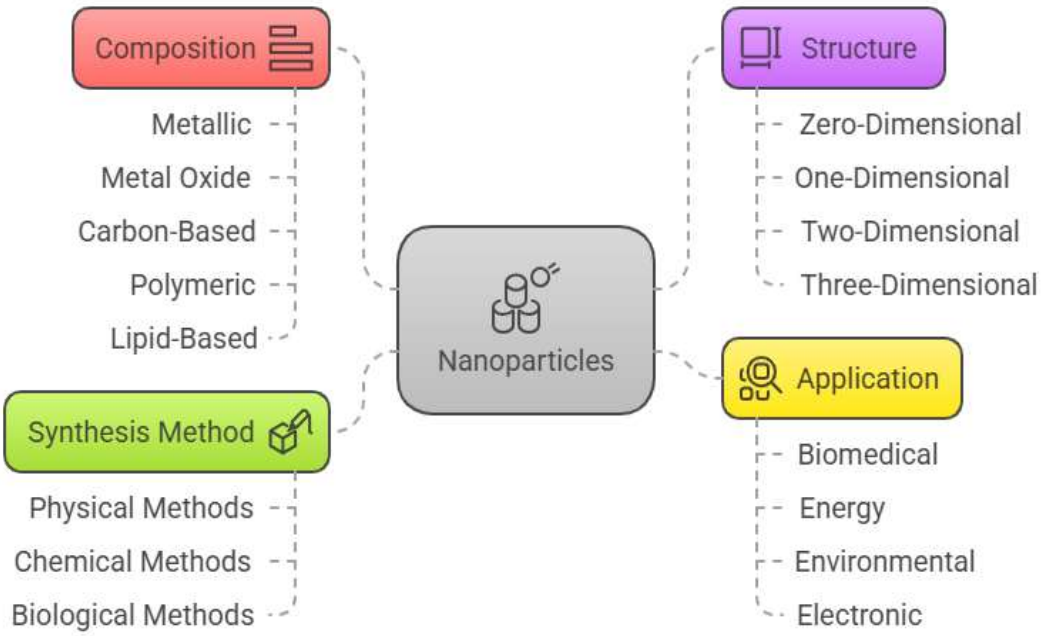

Figure 2.1 Comprehensive classification framework of nanoparticles (Mekuye & Abera, 2023)

2.4 Metal Oxide Nanoparticles

Metal oxide nanoparticles exhibit a range of attractive properties, including high surface area, quantum size effects, and tunable electronic and optical characteristics.

These properties make them suitable for diverse applications in catalysis, electronics, sensing and biomedicine. In particular, their antimicrobial and anticancer activities have garnered significant attention. It is feasible to customize metal oxide nanoparticles' size, shape, and surface chemistry (Bukhari *et al*., 2021).

2.5 Nanoparticles of cobalt oxide and their significance

Cobalt oxide nanoparticles hold substantial relevance owing to their key role in biological systems and specifically as part of vitamin B12. Due to their unique properties, cobalt oxide nanoparticles, can be ideal candidates for anticancer agents. They can address the limitations of traditional treatment options like chemotherapy and radiotherapy. Recent research has shown they selectively inhibit cancer cells, boosting attention towards their synthesis, characterization, and use. This research aims to provide a more effective and safe cancer treatment based on cobalt oxide nanoparticles (Huang *et al.,* 2021)They also have strong antibacterial properties, being active against both gram-negative and gram-positive bacterial, which positions them as alternatives to traditional antibiotics and a new solution to antibiotic resistance (Saeed *et al.,* 2022). They also have uses in water purification and electrocatalysts associated with the oxygen evolution reaction (OER) in the production of clean hydrogen fuel (Dakave *et al.,* 2023). The interest in doping pure cobalt oxide nanoparticles, with other metals (i.e. Zinc and Nickel) relates to the limitations of pure cobalt oxide nanoparticles particularly in terms of their use in biotechnology. Pure cobalt oxide nanoparticles (Co_3O_4) have attractive properties, however their application can be limited by a number of issues relating to stability and electronic properties (Gorylewsky *et al.,* 2025). Due to the limits of pure Cobalt oxide nanoparticles, doping them with transition metals like Nickel and Zinc offers a viable way to improve their characteristics. This strategy not only overcomes the drawbacks of pure Cobalt oxide but also creates new opportunities for its use in catalysis and photocatalysis, among other areas. To advance these doped nanoparticles' useful applications in biotechnology and other fields, more study is needed to create and describe them (Ansari *et al.,* 2025).

2.6 Doping as a strategy for enhancing nanoparticle properties

In response to the ongoing process of integrating nanostructured materials for biological possibility, the modification of cobalt oxide nanoparticles with zinc and nickel offers an interesting biotechnological opportunity (Salah *et al.,* 2011). Cobalt oxide's

electrical properties and catalytic activity can be significantly boosted by doping it with transition metals like Zinc (Zn) and Nickel (Ni), a process that has been thoroughly investigated. For example, Nickel-incorporated Cobalt-rich nanoparticles efficiently coordinated the catalyst's characteristics, particularly in the oxygen evolution reaction (Forsythe *et al.,* 2021). Changes in electrical structure or the appearance of additional putative active sites to aid in the reaction could be the cause of these effects. Additionally, the incorporation of Zinc into cobalt oxide matrices can enhance stability, and its photocatalytic properties show improved activity. Zinc-doped cobalt oxide has indicated and reported enhancing surface area or modifying band gap, both important key properties for photocatalysis (Rana *et al.,* 2022). For cobalt oxide nanoparticles, the enhancement of combining, and doping Zn and Ni would be beneficial for performance specific applications.

i. **Improved bioactivity:** The addition of Zinc and Nickel can lead to alterations in the surface properties of cobalt oxide nanoparticles, and thus the interactions of those nanoparticles in biological systems; cellular uptake, protein binding, and improved biocompatibility (Jiang *et al.,* 2018).
ii. **Targeted drug delivery:** It may be possible to improve direct drug delivery to particular cells or tissues by manipulating the doped nanoparticles' size, shape, and surface chemistry. For instance, drug delivery uses zinc-substituted cobalt ferrite nanoparticles (Vinosha *et al*., 2021).
iii. **Antimicrobial applications:** Both Zinc oxide and Nickel oxide have known antimicrobial properties. These metals can be doped into cobalt oxide to produce nanoparticles with stronger antimicrobial and antifungal capabilities (Zakharova *et al.,* 2019).
iv. **Bioimaging:** Zinc and Nickel doping can modulate Cobalt oxide's magnetic characteristics, making them effective contrast agents in magnetic resonance imaging (Vinosha *et al*., 2021).
v. **Metal Stress Absorbants:** Cobalt oxide nanoparticles can be used for plant growth (Mahmood *et al.,* 2023).

2.7 Synthesis of doped nanoparticles chemically

Zinc and Nickel-doped cobalt oxide nanoparticles are synthesized chemically and biologically**.**

2.7.1 Co-precipitation method: Metal precursors, including cobalt nitrate, nickel sulfate, and zinc nitrate, are precipitated using an appropriate base, usually NaOH or ammonium hydroxide and then calcined in this popular and economical chemical process. By uniformly doping zinc and nickel into the cobalt oxide lattice, this approach allows for the synthesis of nanoparticles with regulated stoichiometry and shape, which is essential for improving the antibacterial capabilities (Naseri *et al.*, 2016).

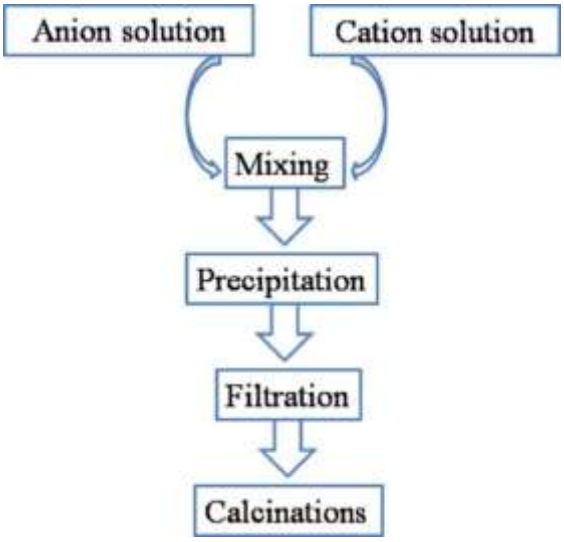

Figure 2.2 Co-precipitation technique steps (Mohammed *et al*., 2023)

Following the co-precipitation approach, Reena and Aslinjensipriya (2023) synthesized pure and Nickel (Ni)-doped Cobalt oxide nanoparticles to assess their optical, structural, and photocatalytic aspects. XRD confirmed a cubic phase with particle sizes ranging from 14 to 22 nm. FTIR identified spinel structure vibrations, while SEM images displayed irregular clusters. EDX confirmed Ni, Co, and O presence. UV-Vis spectroscopy showed a band gap shift toward the visible spectrum. Ni-doped Co_3O_4 exhibited superior MB degradation efficiency under visible light compared to pure Co_3O_4.

Co-precipitation was used to yield Zn-doped CoO_4 (x = 0.05, 0.1, and 0.3) Zn^{2+} inclusion into the Co_3O_4 lattice was verified by XRD. The optical band gap increased as the Zn level increased, according to UV-Vis research. Photocatalytic experiments demonstrated improved breakdown of organic waste, reaching 97% in 120 minutes because to less electron-hole recombination (Reena and Aslinjensipriya (2022).

2.8 Zinc and Nickel-doped Cobalt Oxide Nanoparticles

Combining cobalt oxide with Zinc and Nickel offers a synergistic approach to enhance both antibacterial and anticancer activities. The mechanism of action of Zinc and Nickel-doped cobalt oxide nanoparticles against bacteria and cancer cells involves several interconnected physicochemical and biological processes.

2.8.1 Improved antimicrobial activity: ZnO and NiO both exhibit antibacterial properties, and their combination with Co_3O_4 can broaden the spectrum of activity and enhance the overall antimicrobial effect (Khalid, 2021).

2.8.2 Anticancer effects operate with unison: The distinct mechanisms of action exhibited by ZnO, NiO, and Co_3O_4 have the potential to engender synergistic anticancer effects, thereby enhancing the overall efficacy of oncological treatments (Almoneef, 2024).

2.8.3 Biomedical application: Zinc and Nickel-doped Cobalt oxide nanoparticles have surfaced as promising candidates for antibacterial applications, attributed to their superior physicochemical properties and their capacity to effectively combat bacterial pathogens. The doping process induces modifications in the structural, electronic, and surface attributes of Cobalt oxide nanoparticles, thereby amplifying their antibacterial efficacy (Almoneef, 2024).

2.9 Biological applications

2.9.1 Applications in biomedicine: Zinc and Nickel-doped Cobalt oxide nanoparticles exhibit significant antibacterial efficacy and may be integrated into the formulation of wound dressings to offer protection against multidrug-resistant bacterial strains. Their utilization is further applicable to the coatings of medical instruments, including implants and catheters, thereby markedly diminishing the likelihood of biofilm development and nosocomial infections (Jana *et al.,* 2016).

2.9.2 Purifing of water : The aforementioned nanoparticles can be proficiently utilized within water treatment methodologies, functioning as disinfectants that eradicate waterborne pathogens, attributable to their formidable antibacterial properties (Farhat *et al.,* 2014).

2.9.3 Food packaging: The incorporation of these nanoparticles in food packaging is poised to impede microbial proliferation, thus prolonging the shelf life of perishable commodities by leveraging their intrinsic antibacterial characteristics (Naseri *et al.,* 2016).

2.9.4 Applications in agriculture: Zn and Ni-Co_3O_4 nanoparticles can be utilized as nanofertilizer and as biocides to shield crops from bacterial infections while reducing the need for chemical pesticides. It gives crops a sense of sustainability (Kulandaivel & Hemalatha, 2022).

2.9.5 Antibacterial efficacy

The antibacterial properties exhibited by Zn and Ni-doped Co_3O_4 nanoparticles are ascribed to several mechanisms that disrupt bacterial cellular processes. A significant mechanism encompasses the liberation of reactive oxygen species (ROS). The incorporation of Zinc and Nickel into cobalt oxide enhances the capacity to produce ROS, including hydroxyl radicals (OH^-) and superoxide anions (O_2^-), which provoke oxidative stress within bacterial cells. This oxidative stress leads to lipid peroxidation, protein denaturation, and DNA damage, ultimately culminating in cellular demise (Khan *et al.,* 2023). Another critical mechanism involves membrane disruption, wherein Zn and Ni-Co_3O_4 nanoparticles engage in electrostatic interactions with the bacterial cell membrane. This interaction undermines membrane integrity, resulting in the efflux of intracellular constituents such as proteins and ions. Importantly, Nickel doping amplifies this bactericidal effect by augmenting both the surface charge and reactivity of the nanoparticles (Ali *et al.,* 2022). Furthermore, the liberation of metal ions, specifically Zinc and Nickel, plays a substantial role in the antibacterial efficacy. These ions disrupt the metabolic and enzymatic processes of bacteria. By attaching to nucleic acids, zinc ions prevent DNA replication, whereas nickel ions impede with key enzymatic processes vital to bacterial life (Patil *et al.,* 2021).

2.9.6 Anticancer activity of Cobalt Oxide nanoparticles

Through a variety of ways, Cobalt oxide nanoparticles demonstrate strong anticancer effects. One of the primary actions is the induction of apoptosis, where Co_3O_4 nanoparticles trigger programmed cell death in cancer cells by activating specific signaling pathways, particularly the caspase cascade. Studies have reported that these nanoparticles significantly increase caspase-3 activity, a key enzyme responsible for executing apoptosis, thereby promoting cell death in malignant cells while exerting minimal effects on normal, healthy cells (Al Samri *et al.*, 2021). DNA damage, which occurs primarily by the production of reactive oxygen species (ROS), is another important mechanism. Excess ROS levels cause oxidative stress, which harms lipids, proteins, and DNA, besides cellular macromolecules, adding to the overall lethal effects on cancer cells (Khan *et al.*, 2020).

2.9.7 Specific efficacy against brain cancer

Investigations have underscored the potency of cobalt oxide nanoparticles against glioblastoma cell lines, particularly the U87 variant. Empirical evidence suggests that these nanoparticles possess the capability to impede cellular proliferation and trigger apoptotic mechanisms specifically within brain cancer cells, thereby indicating their promise as a targeted therapeutic modality for cerebral neoplasms. The dimensional characteristics and surface modifications of cobalt oxide nanoparticles significantly affect their permeation and therapeutic efficacy within cerebral tissues. Nanoparticles of reduced size exhibiting functionalized surfaces demonstrate enhanced cellular internalization and directed delivery to neoplastic sites, subsequently augmenting their therapeutic potential against brain malignancies (Wahab *et al.*, 2013).

2.10 Limitations of existing studies

A distinct research gap exists in the comparative examination of the anticancer and antibacterial mechanisms exhibited by Zinc and Nickel-doped cobalt oxide nanoparticles. In particular, an exploration into the effects of varying doping concentrations on the cytotoxicity and antimicrobial efficacy of these nanoparticles, in conjunction with their interactions with cellular signaling pathways, may yield valuable insights into the optimization of their therapeutic applications. Further research into the synergistic effects of these dopants on the creation of reactive oxygen species and their influence on cellular stress responses is also a fascinating subject (Bisht and Rayamajhi, 2016).

3. MATERIALS AND METHODS

All of the media and solutions were autoclaved for 15 minutes at 121 ^{o}C and 15 psi of pressure before to use. Before being used, glassware and plasticware were cleaned, autoclaved, and oven dried. Table 3.1, 3.2 and 3.3 illustrates list of equipment's, apparatus and chemicals respectively.

Table 3.1 List of Equipment's

Sr. No.	Equipment	Company
1	Autoclave	Wiseclave WAC autoclave
2	Magnetic Stirrer	Wise Stir R Feedback Control Digital Timer Function
3	Laminar flow	BIOTECH
4	Measuring balance	METTLER TOLLEDO
5	Incubator	Wise Cube Fuzzy Control System
6	Hot plate	Wise Spin Feedback Control Digital Timer Function
7	Dry Oven	Memmert, Japan

Table 3.2 List of Apparatus along with their Composition

Sr. No.	Apparatus	Volume required/ Composition
1	Beakers	500 ml, 250 ml, 150 ml, 100 ml beaker
2	Spatula	Fisherbrand TM Spoonulet TM
3	Conical Flask	500 ml flask, 125 ml flask 250 ml flask, 50 ml flask
4	Petri Dishes	60 mm * 15mm
5	Eppendorf Tubes	Plastic tubes, 1.5 ml
6	Spirit Lamp	90% concentrated Ethanol
7	Micropipette	Acura 825
8	Inoculation loop	Iron metal
9	pH meter	InoLab

Table 3.3 List of Chemicals

Sr. No.	**Chemicals**
1	LB Nutrient Agar
2	Sodium Hydroxide
3	Gram Negative bacteria: *Salmonella, Acinetobacter, Klebsiella , Shigella,*
4	Gram Positive bacteria :Staphylococcus
5	Distilled water
6	70% Ethanol
7	Whatman membrane filter
8	Cobalt Acetate
9	Nickel oxide
10	Zinc oxide
11	pH buffer solution

Methodology

3.4 Synthesis of Zn and Ni-doped Cobalt oxide nanoparticles

Co-precipitation was used to create Cobalt oxide nanoparticles doped with Zinc and Nickel (Kalpana *et al.*, 2017)

3.5 Co-precipitation method

A 10g of cobalt acetate ($C_4H_6COO_4$) was added in 50 ml deionized water (pink color). The precursor solution was stirred continuously at 70^0 C using a magnetic stirrer. Drop by drop, 2M sodium hydroxide solution was added to the precursor solution until the PH reached 11. The precipitate color turns into blue color. The resulting precipitate was stirred for 2h at 70^0 C until brown precipitate obtained as shown in figure 3.1. For doping 3% Nickel oxide and 3% Zinc oxide was added in solution in separate beaker to obtain doped particles.

$$2Co\ (CH_3COO)_2 + 2NaOH \rightarrow CoO + 2CH_3COONa + H_2O$$

$$6CoO \rightarrow O2 + 2Co_3O_4$$

3.5.1 Washing and drying

The precipitate was washed multiple times with deionized water to remove any residual ions. With the help of filter paper and funnel the washed precipitate was incubated for 2 days to complete dry then the dried powder was crushed in mortar and Pastel

3.5.2 Calcination

For one hour, the dried powder was calcined at 3500 C in a dry oven. Both Nickel-doped Cobalt oxide nanoparticles and pure Cobalt oxide are black. The particles doped with Zinc had a brown hue (Kalpana *et al.*, 2017).

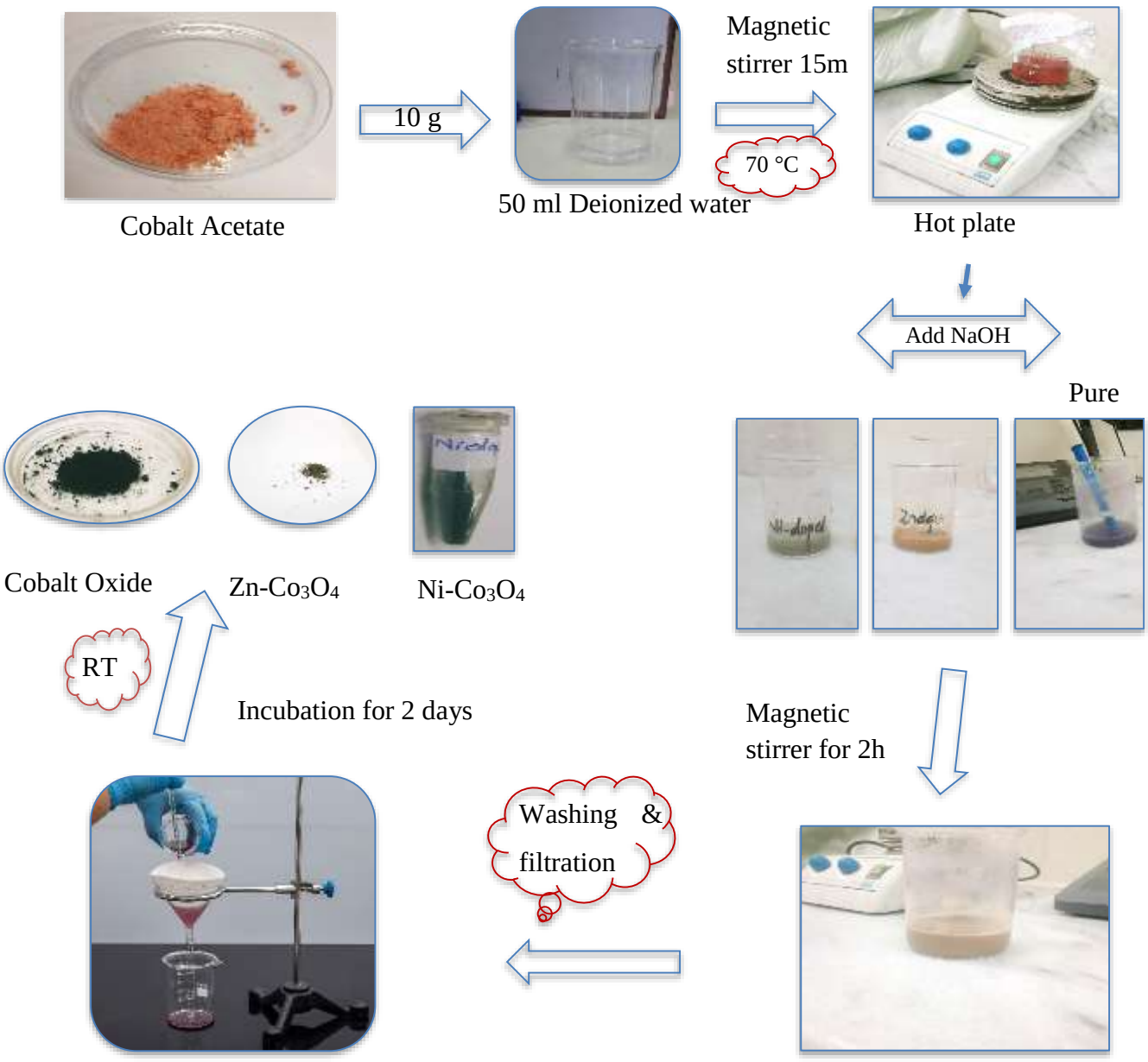

Figure 3.1 Cobalt oxide nanoparticle synthesis using the co-precipitation method (Wang & Kuo, 2013)

3.6 Characterization techniques

The cobalt oxide nanoparticles doped with Zinc and Nickel (Co_3O_4) underwent an extensive examination through a diverse set of analytical techniques, such as UV-Visible spectroscopy (UV-Vis), Fourier Transform Infrared Spectroscopy (FTIR), Scanning Electron Microscopy (SEM), and X-ray Diffraction (XRD), aimed at intricately studying their structural, morphological, and optical traits (Holder, 2019).

3.6.1 X-ray Diffraction (XRD)

Purpose: Identifies the nanoparticles' phase and crystal structure

The crystalline structure of the synthesized nanoparticles was investigated using an X-ray diffractometer (Analytik Jena, Germany). The powdered sample was evenly spread onto the sample holder without any binder. XRD patterns were recorded over a 2θ range of 20°–80°, operating at 40 kV and 30 mA with Cu Kα radiation (λ = 1.5406 Å). The obtained diffraction peaks were analyzed to determine the crystalline phase, structure, and average crystallite size of the nanoparticles. For crystalline materials, this periodicity produces unique diffraction patterns that are represented by many peaks in XRD graphs. Amorphous materials, on the other hand, have XRD graphs with a single wide peak as they don't have a regular atomic structure (Ali, 2022).

3.6.2 Scanning Electron Microscopy (SEM)

Purpose: Investigates the surface morphology and size of nanoparticles.

The scanning electron microscope uses a focused beam of very high energy electrons to produce detailed images of a sample's surface. The interaction of electrons with the sample generates signals such as secondary electrons and backscattered electrons, which provide information about surface topography, morphology, and elemental composition. SEM is extensively used in biology, materials science, and nanotechnology to examine the minute details of complex structures and characterize materials (Akhtar, 2018).

3.6.3 UV-Visible Spectroscopy

Purpose: This is used to study the absorption behavior and energy bandgap.

The optical characteristics of the synthesized nanoparticles were evaluated using a UV–Visible spectrophotometer (Analytik Jena, Germany). To obtain a stable suspension, a small quantity of nanoparticle powder was dispersed in deionized water through Ultra sonication. The absorption spectra were recorded within the 200–800 nm wavelength range using quartz cuvettes. Deionized water was used as a baseline reference for correction. Distinct absorption peaks were analyzed to confirm the synthesis and optical properties of the nanoparticles (Rami & Patel, 2023).

3.6.4 Fourier Transform Infrared Spectroscopy (FTIR)

Purpose: It identifies functional groups and chemical bonding in the nanoparticles.

FTIR analysis was performed using a Shimadzu (Japan) FTIR spectrophotometer equipped with an ATR accessory. Approximately 1–2 mg of dried nanoparticle powder was directly placed onto the ATR crystal, ensuring proper contact using the pressure arm. Spectra were recorded in the range of 4000–500 cm^{-1} with a resolution of 4 cm^{-1} and 32 scans per sample. Background correction was performed before each measurement. The obtained spectra were analyzed to identify characteristic functional groups and metal oxygen bond vibrations (Patel & Patel, 2014).

3.7 Antimicrobial activity

Bacterial strains (*Salmonella, Acinetobacter, Staphylococcus and Klebsiella*) were revived from glycerol-preserved stocks by plating them onto nutrient agar plates. One loop full of 24-hour-old cultures was suspended in 0.1 mL of autoclaved distilled water. The disk diffusion method was used to assess the samples' antibacterial activity (Geoprincy *et al.*, 2011). The bacterial suspensions were spread onto nutrient agar plates using a sterile L-rod spreader. After a 5-minute incubation period, Test samples, dissolved in distilled water to a concentration of 20 to 100 µg/µl each, and were loaded into separate wells, while distilled water alone served as the control. The plates were then incubated at 37°C in incubator for 24 hours. The antibacterial activity was assessed by measuring the diameter of the zone of inhibition surrounding each well, using an antibiotic zone scale.

3.7.1 Media preparation

Five hundred milliliters of deionized water, is filled in 1L Erlenmeyer flask and added 15g of weighed Luria-Bertani (LB) agar powder (Miller, Difco TM). Add a magnetic

stirring bar and mix to make sure all of the powder dissolves. Both the aluminum foil and the autoclave tape are used to seal the flask's top. Next, the flask is placed inside the autoclave and allowed to autoclave for two hours (Cycle P13) at 121 °C, pressure is 15 lbs for 15 min (Ali *et al.,* 2023). It is important to wear autoclave gloves throughout this process. After the autoclave is finished, the flask is taken out (autoclave gloves are needed) and cooled for a maximum of fifteen minutes. When the medium has sufficiently set, the sterilized Petri plates are filled with nutrient agar and allowed to cool for fifteen minutes. To prevent water vapour condensation on the medium, the plates were turned upside down and dried in the safety cabinet for one to two hours. Once dry, the plates are gathered, arranged upward, sealed with tape inside a plastic bag, and refrigerated to be use later. Poured media is shown in figure 3.2.

Figure 3.2 Media Pouring

3.7.2 Reactivation of bacteria preserved in glycerol

Select a bacterial colony from a pure culture using an inoculating wire loop in order to restore a pure culture of bacteria from glycerol stock solution which was store at -20ºC Keep the loop hot to sterilize it, but before selecting the colony be careful not to let the loop get too hot as this might denature the microorganisms. Spread the colony on petri plates after it has been selected. We streak the bacteria over nutrient agar plates that are resistant. Place the plates in the incubator upside down and incubate them for 24 hours at 37°C as shown in figure 3.3.

Figure 3.3 *Salmonella* fresh culture growth after 24 hours

3.7.3 Disk diffusion method

The Kirby-Bauer test, sometimes referred to as the disk diffusion method, is a popular method for determining an organism's resistance to antibiotics. On an agar plate that has been infected with the test organism, disks impregnated with antibiotics are placed. The antibiotic produces a concentration gradient as it permeates the agar, which stops the organism's growth around the disk. To ascertain if the organism is susceptible, intermediate, or resistant to the antibiotic, the diameter of the inhibition zone is measured and compared to standard values (Moradpoor *et al.*, 2019) .

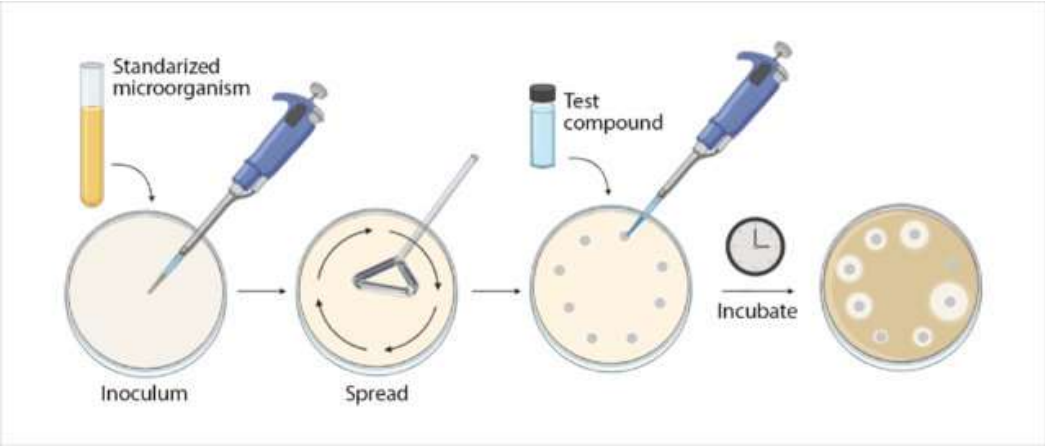

Figure 3.4 Scheme of the agar disk diffusion method (Corrhea *et al*., 2020)

3.8 Anticancer activity

3.8.1 Cell line and culture medium

The U87 brain cancer cell line was cultured in a humidified incubator at 37 °C with 5% carbon dioxide, using Dulbecco's Modified Eagle's Medium (DMEM) supplemented with 4.5 g/L glucose, 10% fetal bovine serum (FBS), and 1% penicillin-streptomycin solution (Khan, 2023). The experiments were conducted in the laboratory of the Atta-ur-Rahman School of Applied Biosciences, National University of Sciences and Technology (NUST), Islamabad, Pakistan.

3.8.2 MTT Assay

A color-based method for evaluating cellular metabolic activity a measure of cell viability is the MTT assay. Using this technique, the yellow MTT dye is changed into purple formazan crystals by metabolically active cells. The number of live cells is exactly proportional to the measured absorbance of the purple color after the crystals have been dissolved. This technique is widely used to measure cytotoxic effects and monitor cell proliferation.

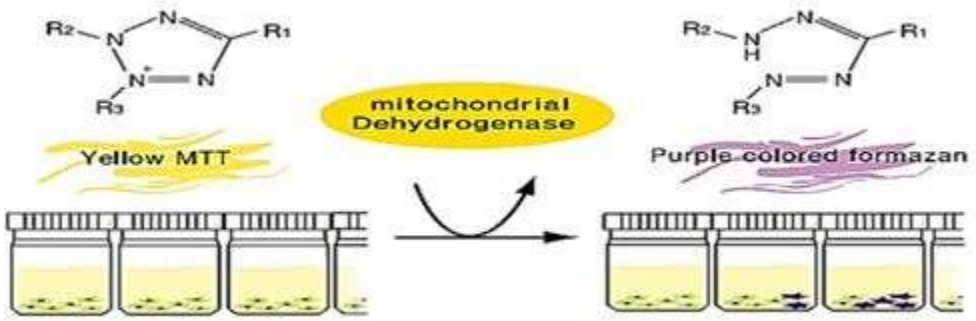

Figure 3.5 MTT assay principle (Vaghela *et al.*, 2022)

For the purpose of promoting cell adhesion, U87 cells were cultivated in 96-well plates at a density of roughly 10×10^3 cells per well and incubated for another night. Later that, the cells were treated with different concentrations of the nanoparticles (100–500 µg/µL) and incubated for 24 hours at 37°C in a humidified atmosphere treated with 5% CO_2. 15 µL of MTT solution 5 mg/mL in PBS (BIO BASIC CANADA INC.) were

added to each well after the treatment time and the plates were incubated for an additional 3 to 4 hours. The growth medium was carefully removed once the incubation was finished, and 100 µL of DMSO was added to dissolve the formazan crystals. A microplate reader (BIO-RAD PR4100) was then used to measure the absorbance at 550 nm. By contrasting the absorbance values of the treated and untreated control cells, cell viability was measured. The percentage of cell survival was determined using the following formula and the obtained absorbance data (Khan, 2023).

$$\% \text{ age of cell viability} = (A_{\text{sample}} - A_{\text{blank}}) / (A_{\text{control}} - A_{\text{blank}}) \times 100$$

4. RESULTS

4.1. Preparation and Characterization of Cobalt oxide nanoparticles doped with Zinc and Nickel oxide

In the current investigation, Cobalt oxide nanoparticles doped with Zinc and Nickel were synthesized utilizing the co-precipitation method, with deionized water serving as the solvent. Throughout the synthesis process, Cobalt ions underwent co-doping with Zinc and Nickel ions, resulting in the generation of Cobalt oxide nanoparticles. The color of the solution exhibited a transition from a pale blue hue to a deeper shade, signifying the successful production of the doped nanoparticles over the duration of the experiment. Characterization methodologies were implemented to evaluate the morphology, physical properties, and chemical composition of the synthesized nanoparticles. The formation and stability of the Zinc and Nickel-doped cobalt oxide nanoparticles were systematically monitored utilizing UV–VIS spectrophotometry. The analysis conducted via UV-visible spectroscopy unveiled a pronounced absorption peak at approximately 250 nm, which is indicative of Cobalt oxide, and this peak exhibited an increase over the incubation period, thereby corroborating the successful doping and synthesis of the nanoparticles. The reduction of metal ions along with the establishment of the cobalt oxide matrix was further substantiated through X-ray diffraction (XRD) analysis. The XRD patterns revealed clear peaks that matched the Cobalt oxide crystal structure, suggesting that the doping of Zinc and Nickel was successful. Additionally, Scanning Electron Microscopy (SEM) was used to examine the shape and size distribution of the nanoparticles.

4.1.1. Optical absorption study

UV-Visible spectroscopy is a useful characterisation method that examines the optical absorption behavior of target nanoparticles to reveal information about their size, shape, and surface features. Figure 4.1 illustrates the absorption spectrum of pure Zn and Ni doped Co_3O_4 nanoparticles respectively. The UV-Visible spectral analysis of the

synthesized nanoparticles displayed distinct absorption peaks within the range of 300–400 nm , the spectrum plots absorbance (in%) against wavelength (in nm). The substitution of Ni ion on the surface of Co_3O_4 nanoparticles results in a wide absorption peak at 316 nm while Zn at 305nm. The UV–Vis absorption spectra demonstrate strong absorbance in the UV region for all samples, confirming their semiconducting nature. In the visible region (450–800 nm), the spectra of pure Cobalt oxide, Zn and Ni-doped Co_3O_4 nanoparticles show significant overlap. Possible causes of overlaping is broadening of absorption bands due to particle size distribution and doping-induced lattice distortions. On the other hand, the Ni-doped sample exhibits broader and more intense absorption across the visible region as compare to Zn-doped cobalt oxide. This can be associated with the presence of defect states or electronic transitions introduced by Ni^{2+} ions, leading to a slightly reduced band gap. As a result, Ni doping enhances visible light absorption, while Co and Zn samples maintain similar optical profiles with overlapping spectra in the visible region.

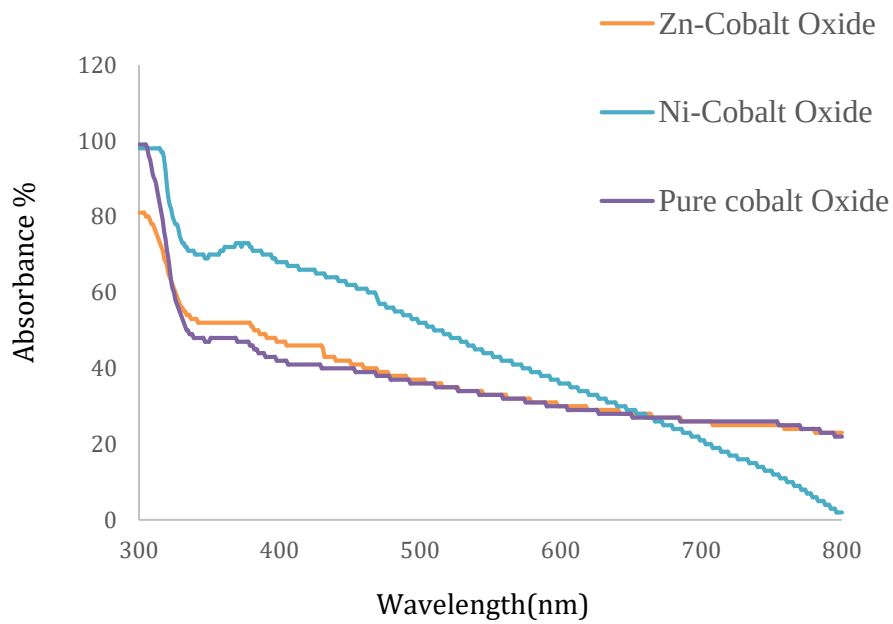

Figure 4.1 UV-Vis Analysis

Using the absorption edge, the band gap (E_g) energy was calculated which is defined as the wavelength at which a sharp increase in absorbance occurs, was identified from the spectrum. By applying the equation $E_g = 1240/\lambda$ which relates the photon energy to the corresponding wavelength.

Undoped Co_3O_4 nanoparticles showed a band gap of 3.46 eV. Upon the incorporation of Zn as a dopant, the energy band gap was observed to diminish to 3.35 eV, thereby indicating a red shift phenomenon. In contrast, the introduction of Ni as a dopant resulted in a further reduction to 3.34 eV, signifying an additional, albeit minor, red shift. These observed variations are attributable to the lattice distortion engendered by the integration of dopants, which subsequently modifies the orbital interactions between cobalt and oxygen atoms, in addition to the emergence of impurity states within the energy band gap that decrease the photon energy requisite for electronic excitation. This meticulous modulation of the energy band gap enhances the prospective applications of doped Co_3O_4 nanoparticles in advanced photocatalytic and optoelectronic domains. The optical characteristics of these materials are instrumental in the generation of reactive oxygen species (ROS), which are recognized to play a significant role in the antibacterial mechanisms associated with metal oxide nanoparticles. The extensive band gap of the synthesized nanoparticles enables effective electron excitation under UV–visible light, thereby facilitating the generation of reactive oxygen species (ROS) such as hydroxyl and superoxide radicals. These reactive species are integral to the antibacterial efficacy observed, as they disrupt bacterial cell membranes and compromise internal cellular structures.

4.1.2. XRD analysis of pure Cobalt oxide Zn and Ni-doped Cobalt oxide nanoparticles

In the present investigation, the crystallite dimensions of synthesized undoped Co_3O_4 were compared with those of Zn and Ni-doped Co_3O_4 nanoparticles utilizing X-ray diffraction (XRD) analysis. XRD examination of the generated metal-doped Co_3O_4 nanoparticles disclosed distinctly defined diffraction peaks, signifying a substantial degree of crystalline order within the material. The crystallite size of metal-doped

Co_3O_4 was determined employing the Scherrer equation, derived from the XRD diffraction data.

$$D = K\lambda/\beta cos\theta$$

In this mathematical expression, D denotes the crystallite dimensions measured in nanometers, K signifies the shape factor (commonly taken as 0.9), λ represents the wavelength of the X-ray, β indicates the full width at half maximum (FWHM) of the chosen diffraction peak, and θ corresponds to the angle of diffraction. The peak corresponding to the most intense plane (440) was used for the estimation of the average crystallite size of Co_3O_4 is ≈ 14.2 nm. The patterns produced by XRD show strong, prominent, and sharp diffraction peaks, showing that the prepared Co_3O_4 nanoparticles have a cubic crystal structure indicate diffraction peaks at 33.73°, 36.73°, 38.20˚, 44.45˚, 47.7°, 64.82˚, 77.95˚ corresponding to the miller indices applied to these planes are (220), (311), (222), (400), (511), (440) and (533) confirmed by (JCPDS 43-1003) as shown in figure 4.4. Two extra peaks at 41.4º and 46.8º appear due to the phase change of Co_3O_4 to CoO corresponding to the (101) and (200) planes these peaks was confirmed by (JCPDS#42-1467) and one peak at (29.37) was due to Co_2O_3 (JCPDS #17-1802). XRD patterns of synthesize nanoparticles confirm the successfully synthesize of cobalt oxide (Co_3O_4). XRD patterns shown in figure 4.2 are frequently used to identify the crystalline structure of materials. The diffraction angle is shown by the X-axis (2θ in degrees), where peaks at particular angles signify the existence of crystallographic planes in the sample. The intensity of the diffracted X-rays, or the number of X-rays dispersed by the sample at each angle, is shown by the Y-axis (Intensity in a.u.). Figure 4.2 displays many peaks at distinct 2θ values, signifying distinct crystallographic planes inside the material. The structural characterization of Zn-doped Co_3O_4 nanoparticles, using XRD with a specific X-ray wavelength, also showed distinct and narrow peaks, confirming their crystalline nature (Mayakannan *et al.,* 2023).

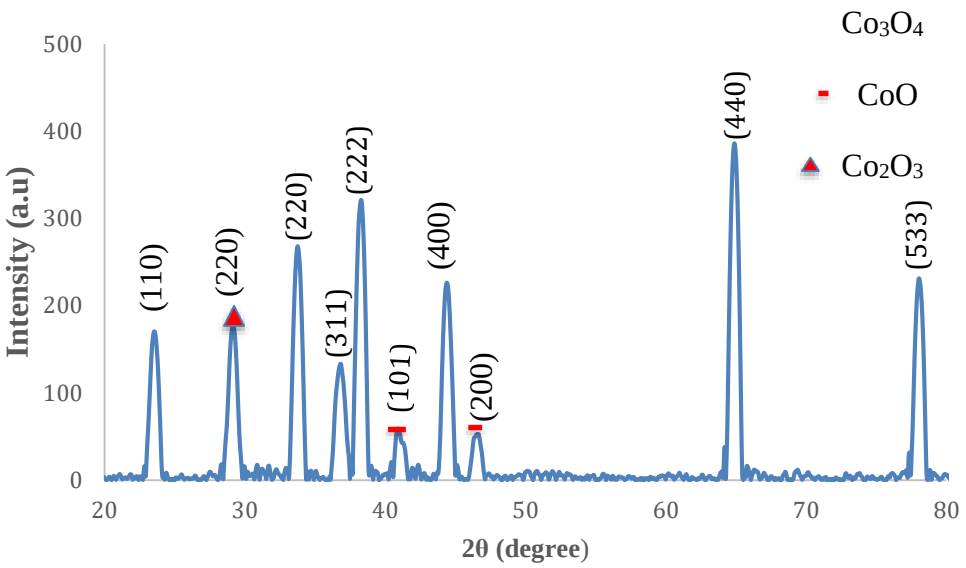

Figure 4.2 X-Ray Diffraction of Cobalt Oxide

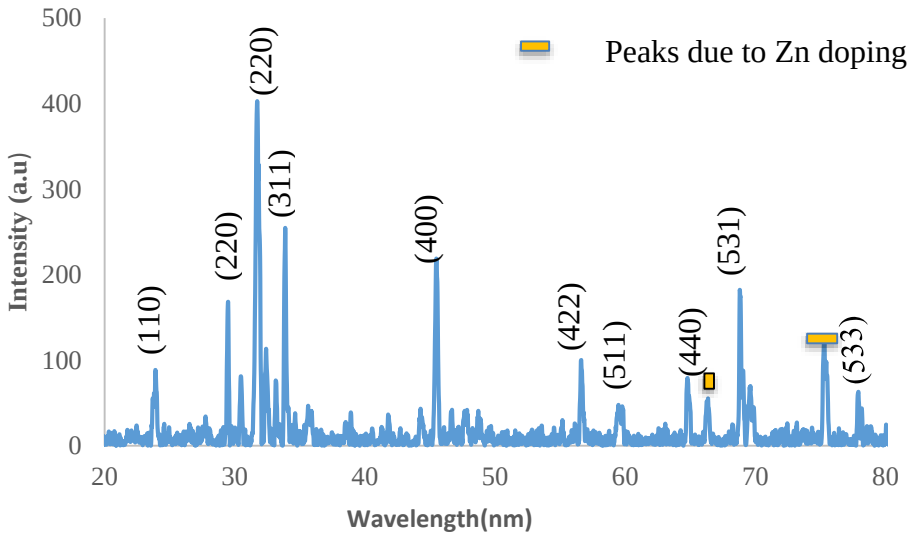

Figure 4.3 X-Ray Diffraction of Zn-Co_3O_4

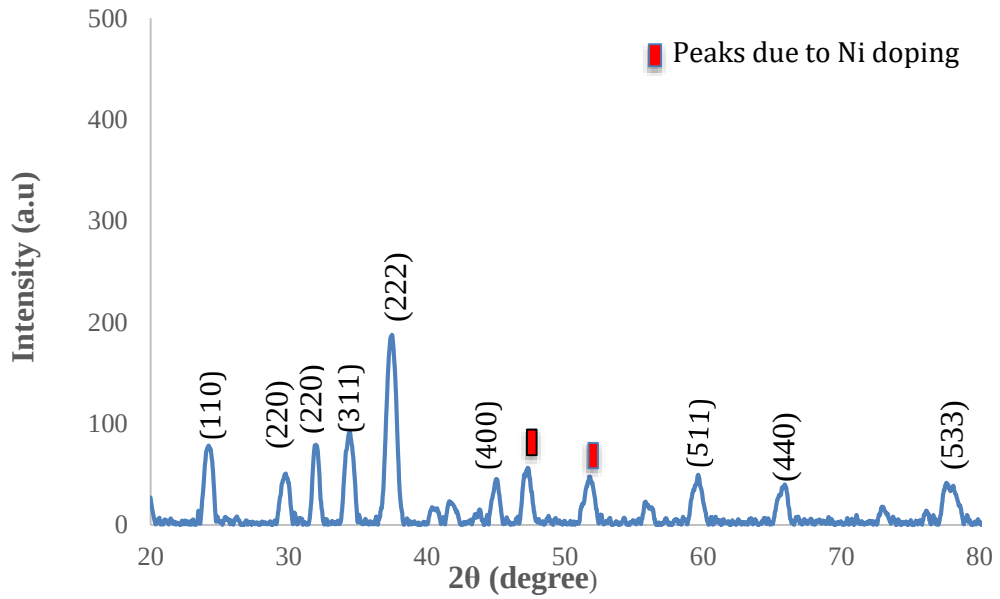

Figure 4.4 X-Ray Diffraction of Ni-Co_3O_4

Figures 4.3 and 4.4 display additional diffraction peaks in the Zn- and Ni-doped Co_3O_4 samples, arising from the incorporation of dopant ions into the crystal lattice. This incorporation induces lattice distortions, localized ordering and in some cases, the formation of secondary spinel-type phases. Such structural changes, commonly reported in doped metal oxides, indicate successful doping and potential enhancements in material properties rather than the presence of impurities (Reena *et al.*, 2022). Crystallite size analysis revealed that the Zn-doped sample, measured at the (220) plane, exhibited an increased size of 23.83 nm, whereas the Ni-doped sample, measured at the (222) plane, showed a reduced size of 10.8 nm, compared with 14.2 nm for pure Co_3O_4. The absence of diffraction peaks corresponding to Zinc or Nickel confirms that their concentrations in the doped materials were below the detection limit of the XRD technique (Zhang *et al.*, 2015).

4.1.3 FTIR Analysis

FTIR spectroscopy provides valuable insights into the chemisorbed species, elemental composition, and the presence of various functional groups within a material. It also reveals information about incoming and outgoing species that may exist on the material's surface. In the FTIR spectrum, a wide range of peaks between 500 and 4000 cm^{-1} is observed, indicating the presence of different functional groups and chemisorbed species in both undoped and Zn doped samples (Rana & Singh, 2016). Absorbed radiation is converted into vibration energy by sample molecules. The detector detects and represents signals as spectrum providing the end result of the molecular fingerprint of the sample.

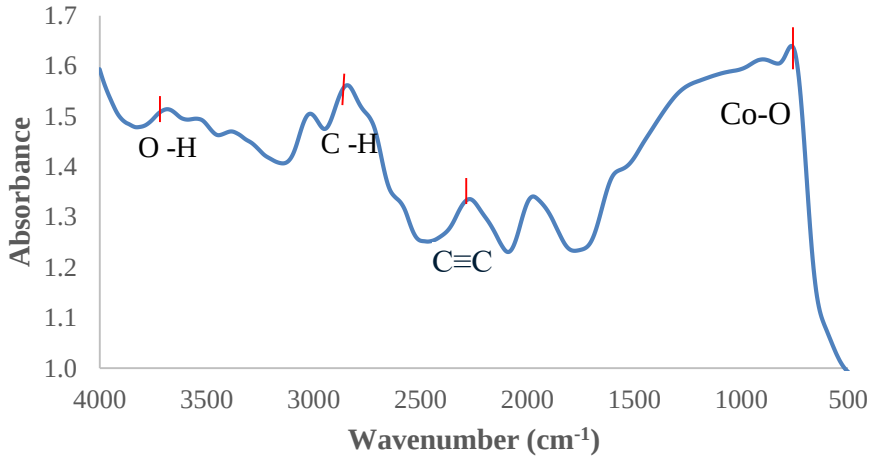

Figure 4.5 FTIR absorbance spectrum of Co_3O_4

Peaks below 1500 represented the fingerprint region and confirmed successful nanoparticles formation. As seen in figure 4.5, vibrations in the graphs reveal that different segments at different levels give different peaks. The strong peak at 732 cm^{-1} corresponds to the characteristic Co–O bands associated with metal oxide rocking vibrations, confirming the formation of Cobalt oxide nanoparticles in the cubic phase (Packiaraj *et al.*, 2018). The vibration band at 3667 cm^{-1} attributed to the O–H stretching and bending vibrations, due to adsorbed water molecules. The identification of the obtained Co-O band may confirm the purity of Co_3O_4 NPs. The peak at 2237

cm^{-1} may correspond to C≡C or C≡N stretching, indicating the presence of alkynes or nitriles.

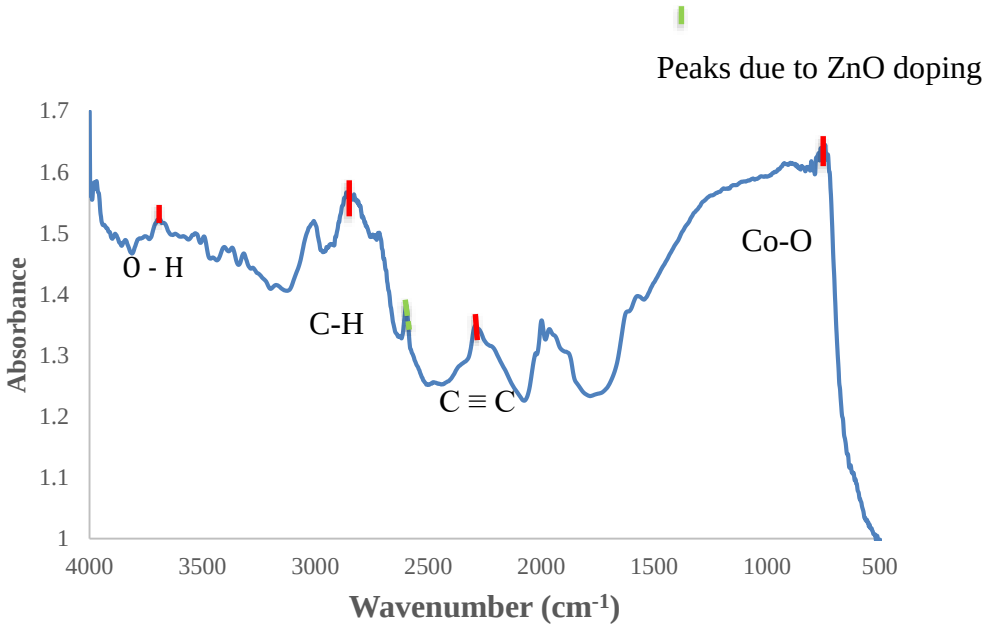

Figure 4.6 FTIR absorbance spectrum of Zn-Co_3O_4

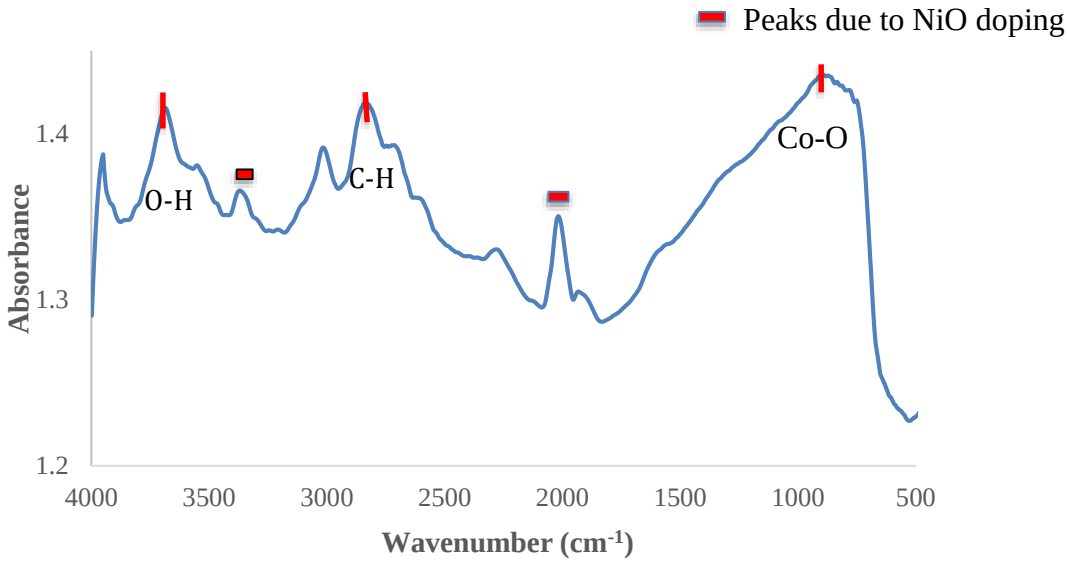

Figure 4.7 FTIR absorbance spectrum of Ni-Co_3O_4

Figure 4.6 show peak at 2597 which confirm Zn dopind and 4.7 illustrate additional absorption bands at 2002 cm^{-1} and 3335 cm^{-1} were attributed Ni , affirming the presence of dopant metals which is absent in pure cobalt oxide (Mayakannan *at al.*, 2020) Absence of any extraneous peaks confirmed the high purity of the synthesized nanoparticles.

4.1.4 SEM Analysis

The SEM shows the distribution of particle sizes and shapes in a sample of nanomaterials. Figure 4.8 left depicts the surface features and particle distribution by illustrating scattered particles exhibiting varying degrees of granularity. The nanometer values shown in the SEM images denote the calculated particle sizes, verifying the nanoscale nature of the synthesized particles. The difference in particle size among pure, Zn-doped, and Ni-doped cobalt oxide is mainly due to the ionic size of the dopants and their effect on crystal growth. Zinc ions, being similar in size to cobalt, cause minimal lattice distortion and promote particle growth, resulting in larger particles (145–239 nm). In contrast, smaller Nickel ions introduce more lattice strain, which restricts crystal growth and leads to smaller particles (110–137 nm).

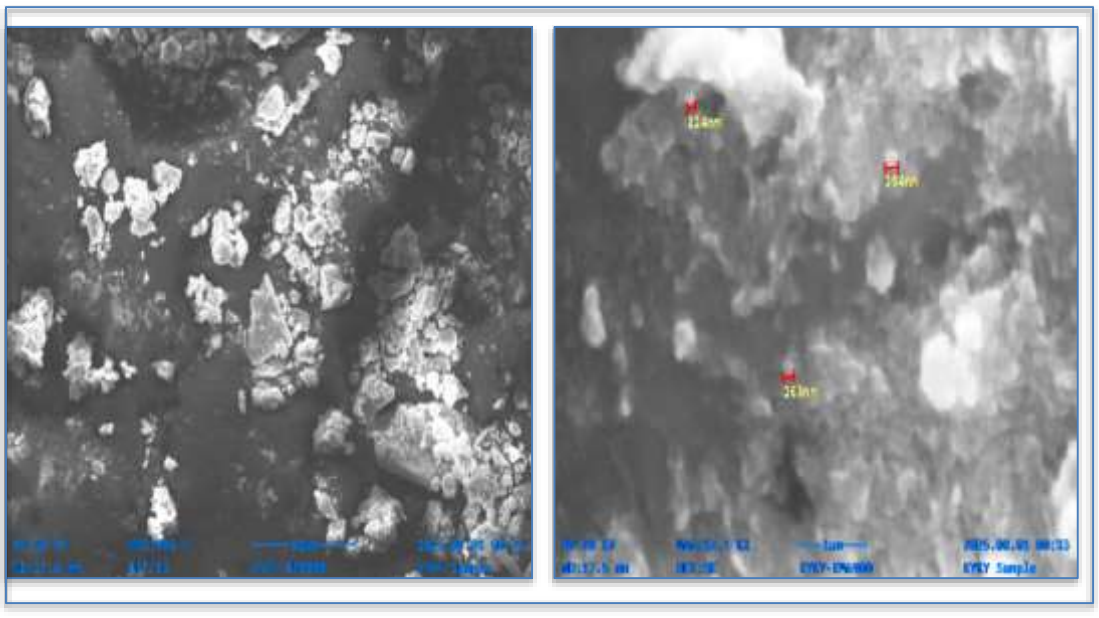

Figure 4.8 SEM analysis of Cobalt Oxide NPs at different magnification (30-1000X)

Figure 4.9 SEM analysis of Zn-Cobalt Oxide NPs at different magnification (30-1000X)

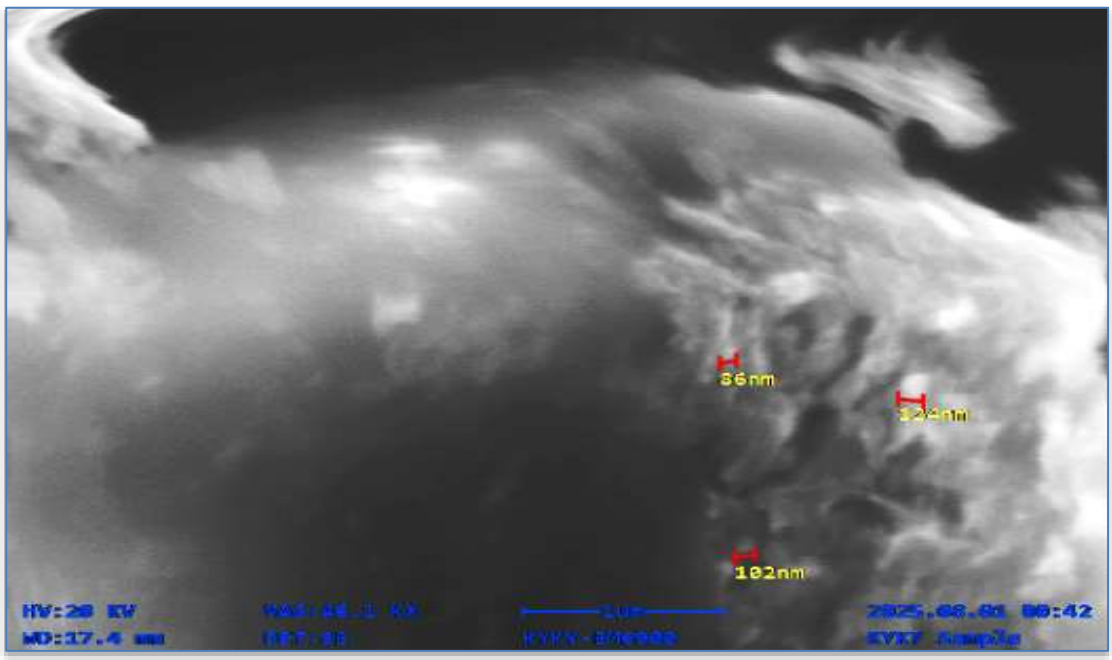

Figure 4.10 SEM analysis of Ni-doped Cobalt Oxide Nanoparticles at different magnification (30-1000X)

4.2 Antibacterial Activity of Zn-doped Co_3O_4 Nanoparticles

The antibacterial activity of Zinc-doped Cobalt oxide nanoparticles was evaluated using the disk diffusion method against *Streptococcus, Klebsiella pneumoniae, Acinetobacter baumannii, Salmonella enterica* and *Staphylococcus aureus* at concentrations of 20–100 µg/µL. For *Salmonella enterica*, inhibition zones increased from 20 mm to 26 mm, plateauing at higher concentrations. *Staphylococcus aureus* showed a clear dose-dependent response, with zones ranging from 5.67 mm to 17.67 mm. *Klebsiella pneumoniae* also exhibited concentration-dependent inhibition, with zones increasing from 3.33 mm to 17 mm. *Acinetobacter baumannii* showed the most variability, with inhibition ranging from 2.3 mm to 3.2 mm and higher standard error, suggesting uneven susceptibility. Error bars representing SE are included in the corresponding graph to visually demonstrate the degree of variation around each mean.

4.2.1 Assessing the impact of Zinc-doped particles on *Salmonella enterica*

This data describes the results of an antimicrobial susceptibility test, showing how different concentrations of a substance inhibit the growth of *Salmonella enterica*. A clear dose-dependent relationship was observed: as the concentration increased from 20 µg/µL to 100 µg/µL, the average zone of inhibition expanded from 6 mm to 22 mm. The most significant increases occurred between 20–80 µg/µL, with only a slight improvement from 20 mm to 22 mm between 80 and 100 µg/µL as shown in figure 4.11. This indicates that the substance is an effective antibacterial agent against *Salmonella*, with its maximum inhibitory effect likely reached near 100 µg/µL (Prashanth *et al.*, 2020).

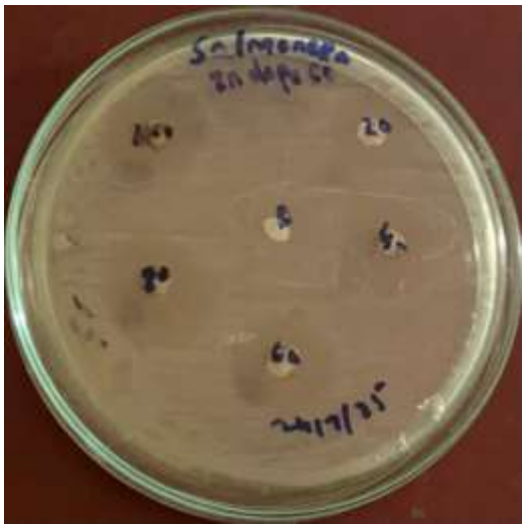

Figure 4.11 Inhibition zone of Zn-Co_3O_4 against *Salmonella enterica*

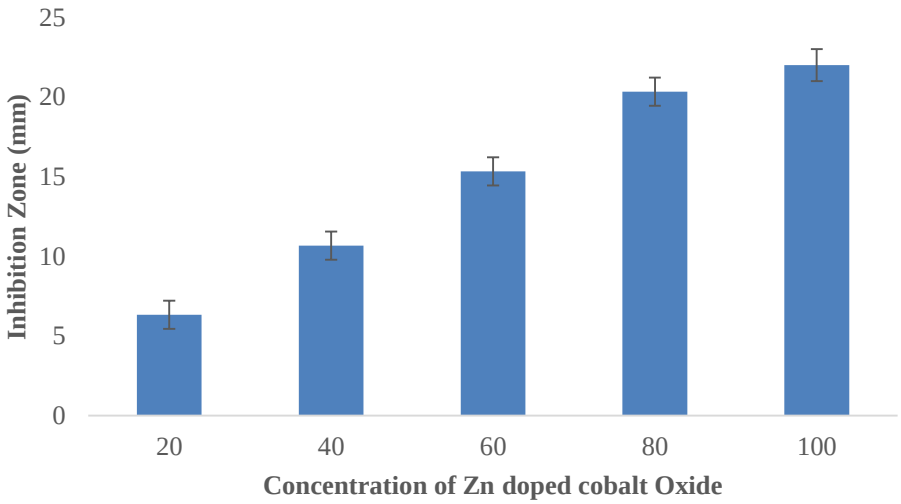

Figure 4.12 Antibacterial activity of Zn-Co_3O_4 against *Salmonella enterica* (bars represent standard error of the mean)

Figure 4.12 demonstrates a dose-dependent antibacterial response of Zinc-doped cobalt oxide nanoparticles against *Salmonella enterica*, with inhibition zones increasing from 6 mm at 20 µg/µL to 22 mm at 100 µg/µL. The strongest activity was observed at higher concentrations (80–100 µg/µL). Standard error (SE) values were generally low, indicating consistent and reproducible results, with slightly more variability at 40 and

60 µg/µL. The included error bars further support the reliability of the findings, confirming the nanoparticles' effective and stable antibacterial performance

4.2.2 Zn-Co_3O_4 NPs Growth Inhibition of *Acinetobacter baumannii*

The antibacterial activity of the tested compound against *Acinetobacter baumannii* was evaluated at concentrations that extend from 20 to 100 µg/µL as shown in figure 4.13. A clear dose-dependent increase in inhibition zones was observed, with mean values progressing from 1 mm at 20 µg/µL to 12 mm at 100 µg/µL. Minimal activity was seen at lower concentrations, but a noticeable improvement occurred from 60 µg/µL onward, where inhibition zones expanded significantly. Variability was higher at lower doses but decreased at higher concentrations, indicating improved consistency and efficacy. Overall, the compound demonstrated moderate but increasing antibacterial activity, with optimal inhibition at 100 µg/µl (Niakan *at al.*, 2010).

Figure 4.13 Inhibition zone of Zn-doped Cobalt oxide against *Acinetobacter baumannii*

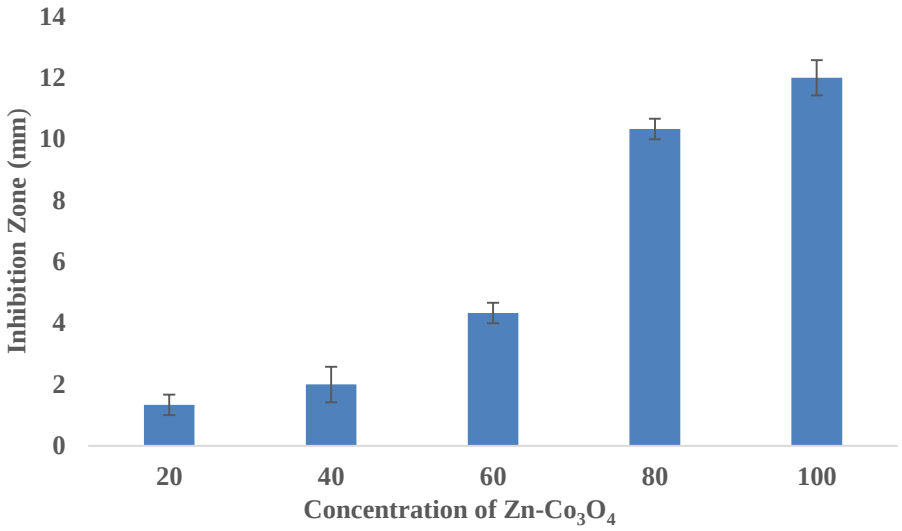

Figure 4.14 Antibacterial activity of Zn-Co_3O_4 against *Acinetobacter baumannii* (bars represent standard error of the mean)

*F*igure 4.14 illustrates the concentration-dependent antibacterial activity of Zinc-doped cobalt oxide nanoparticles against *Acinetobacter baumannii*, with inhibition zones increasing from 1 mm at 20 µg/µL to 12 mm at 100 µg/µL. A noticeable rise in activity begins at 60 µg/µL, where the inhibition zone reaches 4 mm, and continues significantly at higher concentrations. The standard error (SE) values remain relatively low throughout, ranging from 0.33 to 0.58, indicating a good level of consistency and reproducibility in the measurements. Slightly higher variability was observed at 40 µg/µL and 100 µg/µL, but overall the error bars confirm the reliability of the data. These results suggest that Zinc-doped cobalt oxide nanoparticles exhibit increasing and dependable antibacterial efficacy against *Acinetobacter baumannii* at higher concentrations.

4.2.3 Effect of Zn-Co_3O_4 NPs on *Staphylococcus Growth*

The antibacterial activity was assessed at concentrations from 20 to 100 µg/µl as shown in figure 4.15. At the lowest concentration (20 µg/µL), inhibition zones were minimal, suggesting limited antibacterial effect and higher variability among replicates. As the concentration increased to 40 and 60 µg/µL, the inhibition became more pronounced, while at 80 and 100 µg/µL, the zones continued to grow steadily, reaching the maximum average of 14.33 mm at 100 µg/µL. Overall, the results suggest that while

the antibacterial activity of Zinc-doped cobalt oxide nanoparticles against *S. aureus* increases with concentration, the rate of increase is moderate compared to other strains.

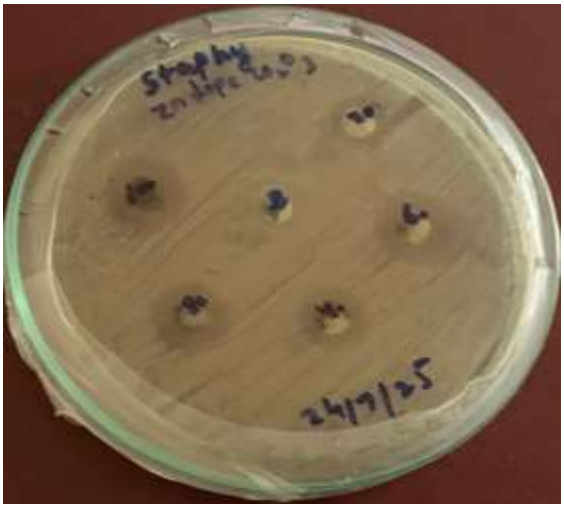

Figure 4.15 Inhibition zone of Zn doped cobalt Oxide against *Staphylococcus Aureus*

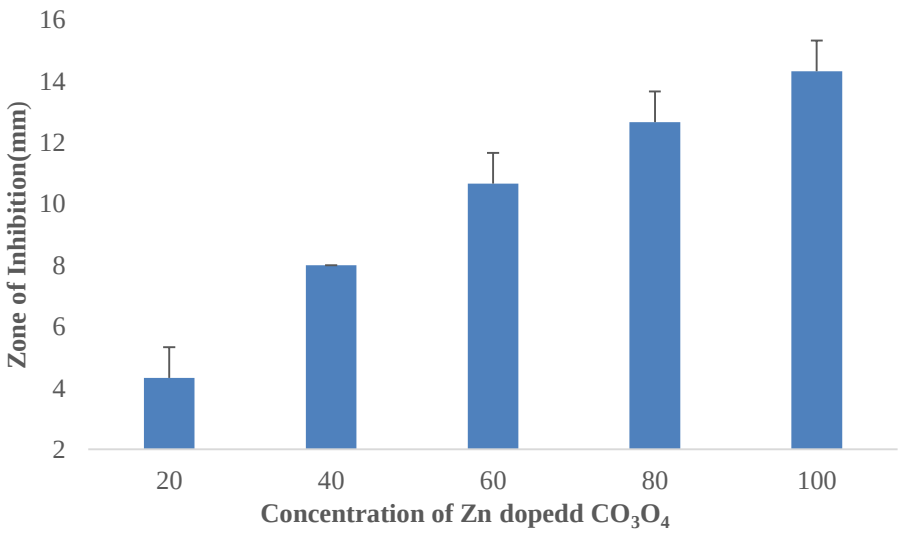

Figure 4.16 Antibacterial activity of Zn-Co_3O_4 against *Staphylococcus aureus (*bars represent standard error of the mean)

Figure 4.16 presents the antibacterial effectiveness of Zinc-doped cobalt oxide nanoparticles against *Staphylococcus aureus* at concentrations of 20 µg/µL, to 100 µg/µL. The mean inhibition zones exhibit a steady rise, starting from 4.33 mm at 20

µg/µL and increasing to 14.33 mm at 100 µg/µL, indicating a clear concentration-dependent antibacterial response. The standard error (SE**)** values show greater variation at lower concentrations particularly at 20 µg/µL indicating less consistent antibacterial performance at minimal doses. However, SE values become smaller and more stable from 40 µg/µL onward, reflecting improved reproducibility and reliability of results at higher concentrations.

4.2.4 Antibacterial potential against *Klebsiella pneumoniae*

The antibacterial response of the tested Zinc-doped cobalt oxide nanoparticles was evaluated across concentrations ranging from 20 µg/µL to 100 µg/µL as shown in figure 4.17. The mean inhibition zones showed a clear concentration dependent increase, starting from 3.33 mm at 20 µg/µL and reaching 17 mm at 100 µg/µL. At the lower concentrations (20 and 40 µg/µL), antibacterial activity was minimal, with mean zones of 3.33 mm and 5.67 mm, respectively, indicating limited initial interaction with the bacterial cells. A more pronounced antibacterial effect emerged at 60 µg/µL and beyond, with inhibition zones increasing to 11 mm, 14 mm, and 17 mm at 60, 80, and 100 µg/µL, respectively. This steady improvement indicates a measurable dose-dependent response, with significantly enhanced efficacy at higher concentrations.

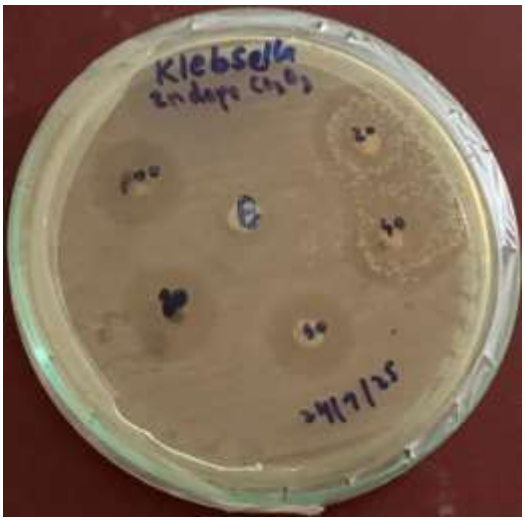

Figure 4.17 Inhibition zone of Zn- doped cobalt oxide *against Klebsiella pneumoniae*

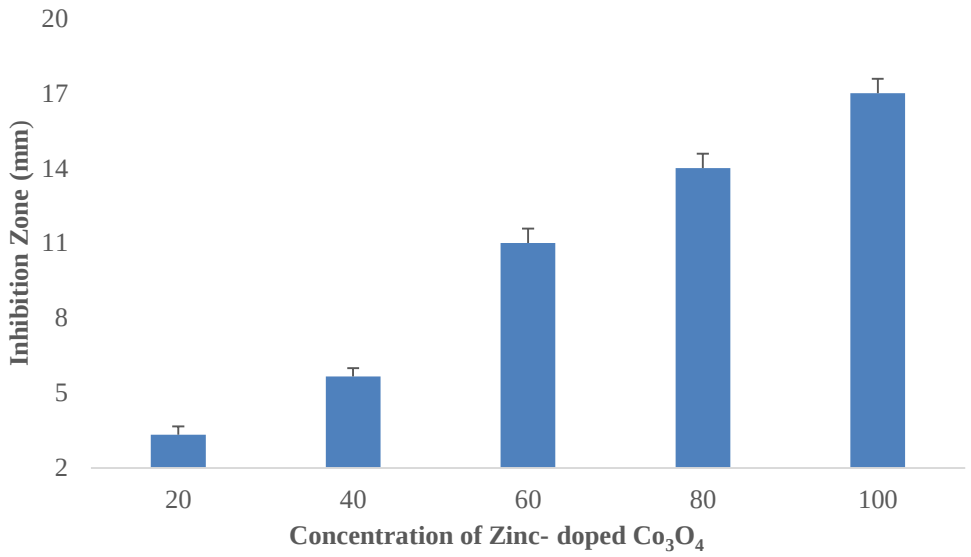

Figure 4.18 Antibacterial Activity of Zn-Co_3O_4 against *Klebsiella pneumoniae(*bars represent standard error of the mean)

Figure 4.18 presents the antibacterial activity of Zinc-doped cobalt oxide nanoparticles against *Klebsiella pneumoniae* at concentrations of 20 µg/µl to 100 µg/µl. The mean inhibition zones show a progressive and dose-dependent increase, starting from 3.33 mm at 20 µg/µl and reaching 17 mm at 100 µg/µl. A more pronounced increase is observed from 60 µg/µl onwards, suggesting enhanced interaction of nanoparticles with bacterial membranes at higher concentrations. The error bars represent the standard error (SE), which was relatively larger at lower concentrations indicating higher variability and less consistent antibacterial response. However, SE values decreased considerably at 60 µg/µl and above, highlighting more uniform and reproducible inhibition zones. This reduction in SE at higher concentrations strengthens the evidence for the reliable antibacterial efficacy of the nanoparticles. Overall, these findings support the potential of Zinc-doped cobalt oxide nanoparticles as effective and consistent antibacterial agents, particularly at concentrations of 60 µg/µl and higher.

4.3 Antibacterial Activity of Nickel-doped Cobalt oxide

The antibacterial activity of Nickel-doped cobalt oxide nanoparticles was assessed using the disk diffusion method against *Streptococcus*, *Klebsiella pneumoniae*, *Acinetobacter baumannii*, *Salmonella enteritidis*, and *Staphylococcus aureus* at concentrations ranging from 20 to 100 µg/µL. For *Salmonella enteritidis*, the mean

inhibition zones increased from 4.67 mm to 12.67 mm, showing a concentration-dependent trend. *Staphylococcus aureus* exhibited no activity at lower doses, but showed significant inhibition from 60 µg/µL onward, with zones rising from 7.00 mm to 12mm. *Klebsiella pneumoniae* demonstrated a gradual increase in inhibition from 3.33 mm to 13.00 mm, with a notable rise beyond 60 µg/µL. *Acinetobacter baumannii* exhibited low and variable inhibition, ranging from 2.00 mm to 6.33 mm, with higher standard error, indicating inconsistent response.

4.3.1 Effects of Nickel-doped Cobalt oxide nanoparticles on *Salmonella enterica*

The antimicrobial susceptibility test conducted against *Salmonella enteritidis* revealed a concentration-dependent response to the tested substance. At the lowest concentration of 20 µg/µL, the mean zone of inhibition was 4.67 mm**,** indicating limited antibacterial activity. A notable increase in inhibition was observed as the concentration increased to 40 µg/µL and 60 µg/µL, with mean zones of 9.00 mm and 8.33 mm, respectively. The inhibition zone expanded further to 12.00 mm at 80 µg/µL, and slightly increased to 12.67 mm at 100 µg/µL. These results suggest that the substance possesses effective antibacterial properties against *Salmonella enteritidis*, with its maximum inhibitory effect approaching saturation near 100 µg/µL as shown in figure 4.19.

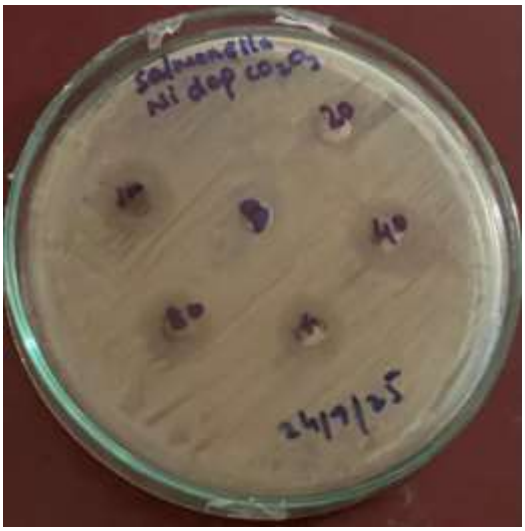

Figure 4.19 Inhibition zone of Nickel-doped cobalt oxide against *Salmonella enteritica*

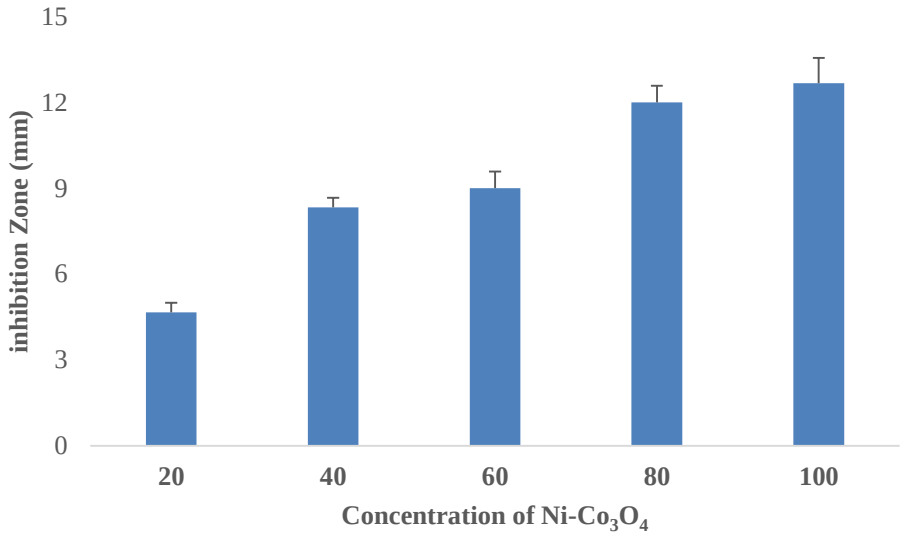

Figure 4.20 Inhibitory effect of Ni-doped Co_3O_4 nanoparticles on *Salmonella enteritidis* (bars represent standard error of the mean)

Figure 4.20 presents the antibacterial activity of Nickel-doped cobalt oxide nanoparticles against *Salmonella enteritidis* at concentrations of 20–100 µg/µL. The mean inhibition zones increased in a concentration-dependent manner, starting at 4.67 mm (20 µg/µL) and reaching 12.67 mm (100 µg/µL). A notable rise in activity occurred from 60 µg/µL onward, indicating enhanced interaction with bacterial membranes. Standard error (SE) was higher at lower concentrations, suggesting more variability, but decreased above 60 µg/µL, reflecting more consistent results. These findings support the reliable antibacterial effect of the nanoparticles at 60 µg/µL and above.

4.3.2 Response of *Acinetobacter baumannii to Ni-doped Nanoparticles*

The antimicrobial activity of the tested substance against *Acinetobacter baumannii* was evaluated across concentrations ranging from 20 µg/µL to 100 µg/µL. A clear concentration-dependent trend was observed, though the increase in inhibition was relatively modest. At 20 µg/µL, the mean inhibition zone was 2.00 mm, indicating weak antibacterial activity at lower doses. This increased to 5.00 mm at both 40 µg/µL and 60 µg/µL, suggesting a threshold level of effectiveness was reached. Further increases in concentration yielded only slight improvements, with inhibition zones of 6.00 mm at 80 µg/µL and 6.33 mm at 100 µg/µL. These findings suggest that while the substance exhibits antibacterial effects against *Acinetobacter baumannii*, its efficacy may be

limited, with only incremental gains observed at higher concentrations as shown in figure 4.21.

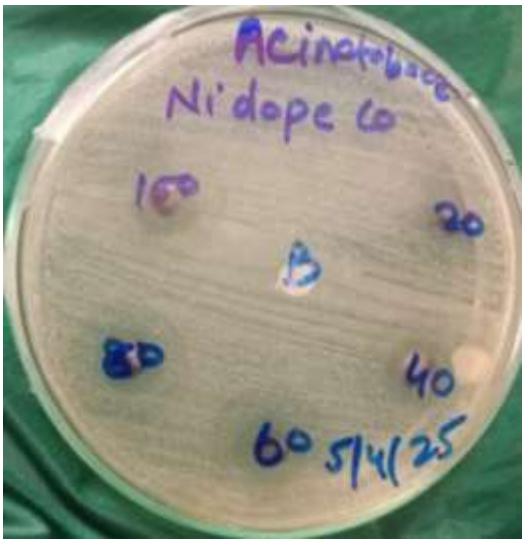

Figure 4.21 Inhibition Zone of Ni-Co_3O_4 against *Acinetobacter baumannii*

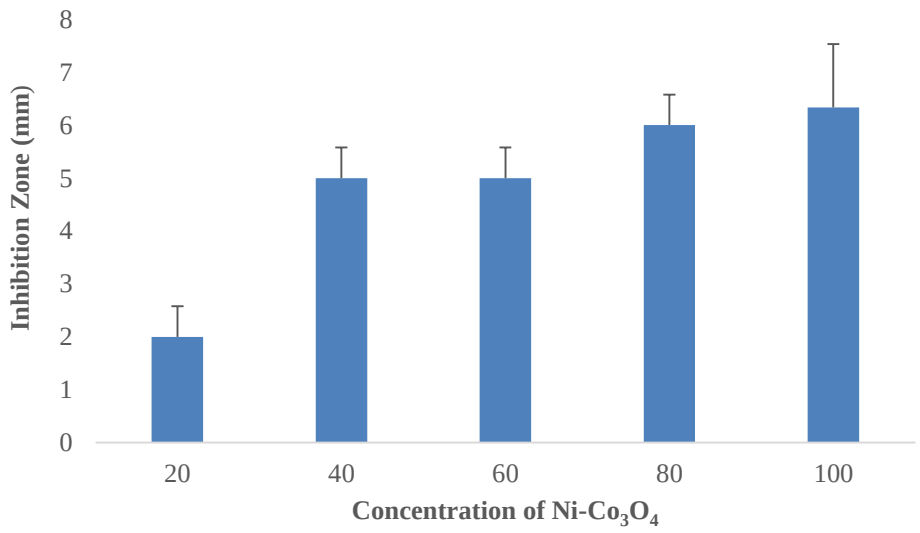

Figure 4.22 Antibacterial activity of Ni-Co_3O_4 against *Acinetobacter baumannii* (bars represent standard error of the mean)

Figure 4.22 illustrates the antibacterial activity of Nickel-doped cobalt oxide nanoparticles against *Acinetobacter baumannii* at concentrations of 20–100 µg/µL. The

mean inhibition zones showed a slight, dose-dependent increase, starting at 2.00 mm (20 µg/µL) and reaching 6.33 mm (100 µg/µL). Moderate activity was observed at 40–80 µg/µL with consistent zones around 5–6 mm. Standard error (SE) was higher at lower concentrations, indicating variability, but became more stable at higher doses. These results suggest limited but gradually improving antibacterial activity, with better consistency above 60 µg/µL.

4.3.3 Bactericidal Effect of Nickel-doped Nanoparticles on *Staphylococcus aureus*

The antimicrobial susceptibility test against *Staphylococcus aureus* demonstrated a distinct concentration-dependent inhibitory response to the tested substance. At the lower concentrations of 20 µg/µL and 40 µg/µL, low antibacterial activity was observed**.** However, a marked increase in activity appeared at 60 µg/µL, where the inhibition zone reached 7.00 mm, indicating the onset of measurable antibacterial effect. This activity further intensified at higher concentrations, with inhibition zones of 10.00 mm at 80 µg/µL and 12.00 mm at 100 µg/µL. These results suggest that the substance begins to exhibit effective antibacterial action against *Staphylococcus aureus* at concentrations ≥60 µg/µL, with its potency increasing steadily thereafter as shown in figure 4.23.

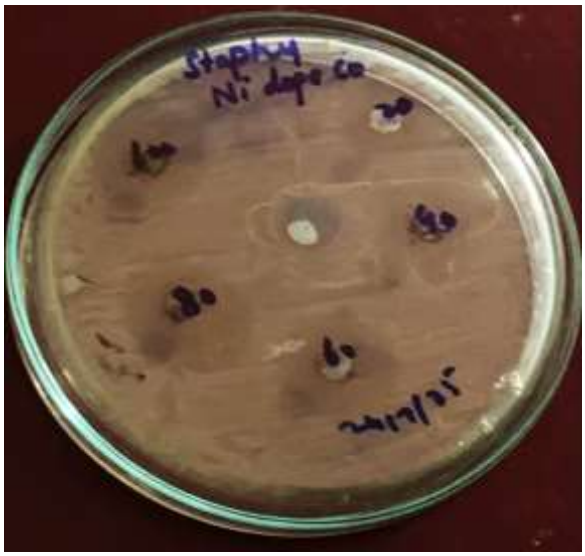

Figure 4.23 *Inhibition Zone of Ni-Co_3O_4 against Staphylococcus aureus*

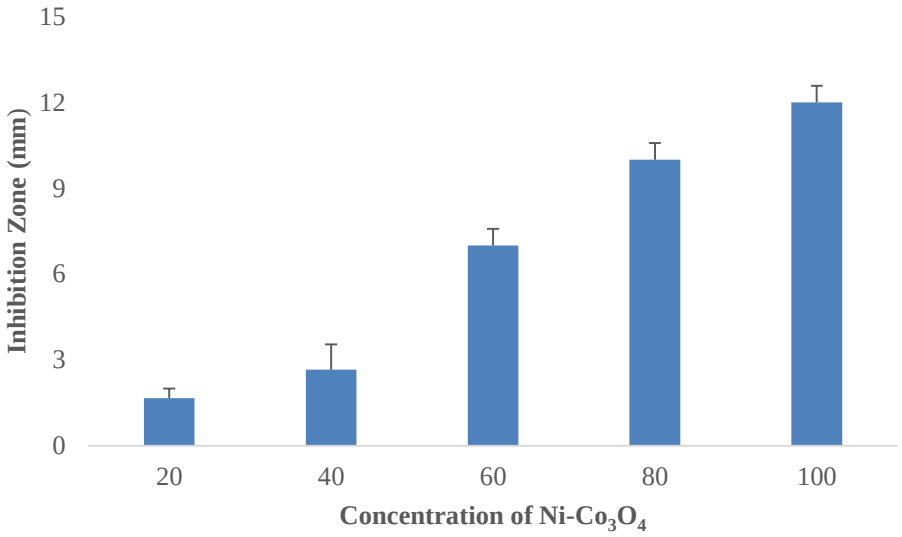

Figure 4.24 Antibacterial activity of Ni-Co_3O_4 against *Staphylococcus aureus* (bars represent standard error of the mean)

Figure 4.24 Ni-Co_3O_4 nanoparticles activity against *Staphylococcus aureus* across concentrations of 20–100 µg/µL. The inhibition zone diameter increased in a dose-dependent manner, from about 1.5 mm at 20 µg/µL to 2.8 mm at 40 µg/µL. A marked enhancement was observed at 60 µg/µL with an average zone of 7.1 mm, further expanding to 10.2 mm at 80 µg/µL and 12.1 mm at 100 µg/µL. Standard error analysis showed greater variability at lower doses, while higher concentrations exhibited more consistent results. Overall, Ni-Co_3O_4 nanoparticles displayed significant and consistent antibacterial activity at concentrations above 40 µg/µL, with strong effects from 60 µg/µL onwards.

4.3.4 Inhibitory Activity of Ni-doped Nanoparticles on *Klebsiella pneumoniae*

The antimicrobial susceptibility test against *Klebsiella pneumoniae* demonstrated a concentration-dependent antibacterial effect of the tested substance. At the lower concentrations of 20 µg/µL and 40 µg/µL, the mean inhibition zones were 3.33 mm and 4.00 mm, respectively, indicating only mild antibacterial activity. A substantial increase was observed at 60 µg/µL, with the inhibition zone widening to 8.67 mm, marking the beginning of a more effective antimicrobial response. Further increases in concentration enhanced the activity, reaching 9.00 mm at 80 µg/µL and peaking at 13.00 mm at 100 µg/µL. These findings suggest that the substance begins to exhibit significant

antibacterial action against *Klebsiella pneumoniae* at concentrations ≥60 µg/µL, with increasing effectiveness at higher doses as shown in the figure 4.25.

Figure 4.25 Zone of Inhibition of Ni-doped cobalt oxide against *Klebsiella pneumoniae*

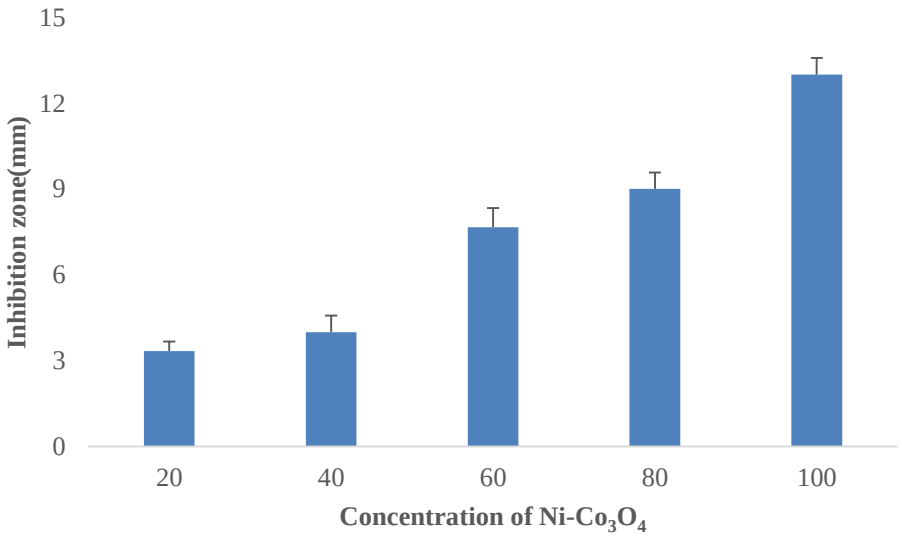

Figure 4.26 Antibacterial activity of Ni-Co_3O_4 against *Klebsiella pneumoniae* (bars represent standard error of the mean)

Figure 4.26 illustrates the antibacterial potential of Nickel-doped cobalt oxide nanoparticles against *Klebsiella pneumoniae* across a concentration range of 20–100 µg/µL. The data reveal a gradual increase in mean inhibition zones, starting at 3.33 mm for 20 µg/µL and reaching 13.00 mm at 100 µg/µL. A more pronounced antibacterial effect becomes evident from 60 µg/µL onwards, with corresponding inhibition zones of 8.67 mm**,** 9.00 mm**,** and 13.00 mm at higher doses. The standard error (SE) was notably greater at lower concentrations, suggesting variability in bacterial response; however, SE values declined with increasing concentration, indicating more consistent and reproducible effects. Overall, the findings point to a concentration-dependent antibacterial response, with effective and stable inhibition beginning at 60 µg/µL.

4.4. Cytotoxicity Assay

To evaluate the anticancer efficacy of Zinc and Nickel-doped cobalt oxide (Zn/Ni-Co_3O_4) nanoparticles, the U87 human brain cancer cell line was utilized from ASAB, NUST Islamabad. The study was conducted at ASAB lab using a range of nanoparticle concentrations 100, 200, 300, 400, and 500 µg/µL. The findings revealed a concentration-dependent cytotoxic response, where increasing nanoparticle doses led to a gradual decline in cell viability. However, beyond a certain concentration, further increases in dosage resulted in only a slight additional reduction in viability, suggesting a potential saturation point in cytotoxic effectiveness.

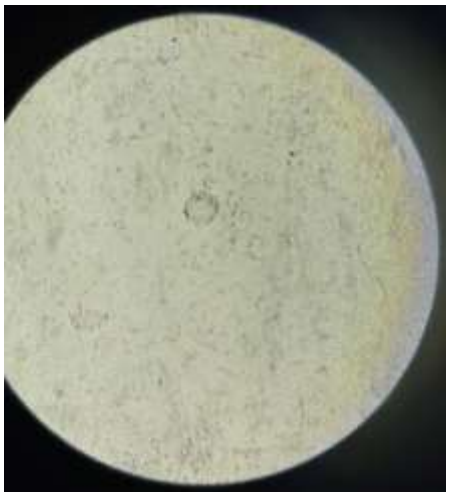

Figure 4.27 Non treated U87 human brain cancer cell lines at 10X magnification

4.4.1 Zinc-doped Cobalt oxide effect on Brain cell line

The anticancer potential of Zinc-doped cobalt oxide nanoparticles was assessed using the U87 glioblastoma cell line. The results revealed a concentration-dependent reduction in cell viability, indicating increased cytotoxicity with rising nanoparticle doses. At lower concentrations (100 and 200 μg/μL), cell viability remained relatively high at approximately 40.26% and 38.59%, respectively as shown in figure 4.28. However, a sharp decline was observed at 300 μg/μL, where viability dropped to just 1.44%, and became negative at 400 and 500 μg/μL, with values of -4.94% and -4.42%, respectively. A clear trend of escalating cytotoxicity was noted as the concentration increased, exceeding 100% at the highest levels. These findings suggest that Zn-Co_2O_3 nanoparticles exhibit strong cytotoxic effects against U87 cells, likely through mechanisms such as reactive oxygen species generation and interference with essential cellular functions.

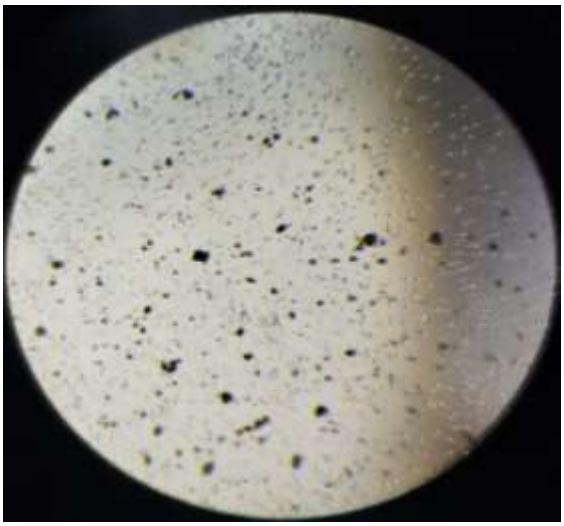

Figure 4.28 Treated U87 Glioblastoma cells against Zn-Co_3O_4 at magnification 10X.

Table 4.1 Zinc-doped Co_3O_4 Nanoparticles' concentration and cell viability

Concentration (µg/µl)	Cell Viability %
100	**40.257**
200	**38.586**
300	**1.4355**
400	**-4.9364**
500	**-4.415**

- Shows complete loss of viable cells

Table 4.1 elucidates the impact of varying concentrations of Zinc-doped Cobalt Oxide nanoparticles on the viability of U87 glioblastoma cells. As Zn-Co_2O_3 concentration decreases from 500 µl to 100 µl, we see a substantial drop in cell viability, demonstrating a toxicity that correlates with dosage. At the highest concentration (500 µl), cellular viability exceeds 100%, implying potential cellular proliferation or negligible toxicity.

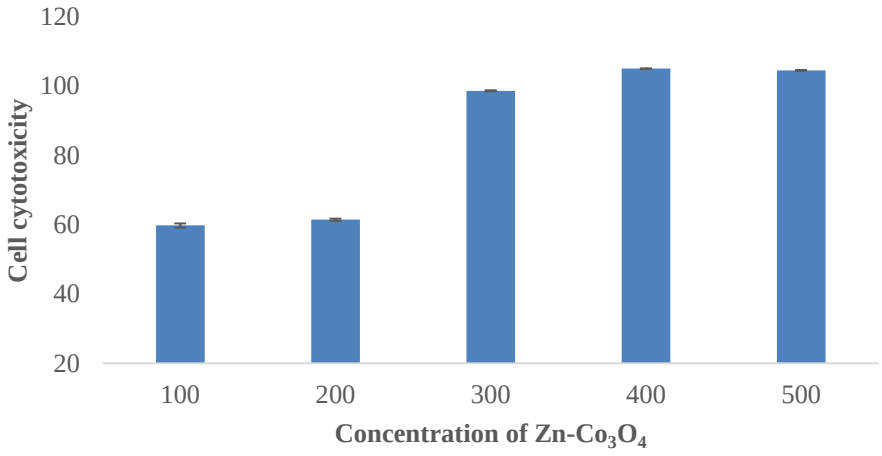

Figure 4.29 U87 glioblastoma cells treated with 100, 200, 300, 400, 500 µg/µl for 24 hours against Zn-Co_3O_4

The Zn-doped Co_3O_4 nanoparticles' cytotoxicity test against the U87 glioblastoma cell line demonstrates a definite dose dependent response. At lower concentrations (100–200 µg/µl), the cytotoxic effect is moderate, with approximately 60% cell death. However, a sharp increase in cytotoxicity is observed at 300 µg/µl, where cell viability drops dramatically, indicating a strong inhibitory effect. This high cytotoxicity is maintained at 400 and 500 µg/µl, with values approaching or exceeding 100%, suggesting near-complete or complete loss of cell viability. These results indicate that Zn-Co_2O_3 nanoparticles exhibit significant anticancer potential at higher concentrations, likely due to enhanced cellular uptake and the induction of oxidative stress or apoptotic pathways in cancer cells.

4.4.2 Nickel-doped Cobalt oxide effect on brain cell line

The anticancer activity of Nickel-doped Cobalt oxide nanoparticles was assessed against the U87 brain cancer cell line across a range of concentrations from 100 to 500 µg/µl. The results revealed a concentration-dependent decrease in cell viability at lower doses, followed by a notable increase at the highest concentration. At 100 µg/µl, the cell viability was approximately 18.22%, and remained low at 200 µg/µl (19.28%), 300 µg/µl (23.28%), and 400 µg/µl (24.43%), indicating strong cytotoxic effects in this range. However, at 500 µg/µl, the cell viability increased significantly to 51.15%, suggesting a possible saturation effect or cellular adaptation at higher doses. These findings demonstrate the potential of Ni-Co_3O_4 nanoparticles to inhibit the proliferation of brain cancer cells, particularly at concentrations below 500 µg/µl, likely due to oxidative stress or disruption of essentialcellularfunctions as shown in figure 4.30 .

$$IC_{50} \approx C1 + \frac{50 - V1}{V2 - V1} \times C2\text{-}C1$$

V_1: Cell viability just above 50% is 51.15% at 500 µg/µl of concentration

1. **V_2:** Cell viability just below 50% is 24.429% at 400 µg/µl of concentration
2. **C_1:** Concentration corresponding to V_1 = 500 µg/µl
3. **C_2:** Concentration corresponding to V_2 = 400 µg/µl

$$IC_{50} \approx 500 + \frac{50 - 51.15}{24.429 - 51.15} \times 500\text{-}400$$

$IC_{50} \approx 121.52$ µg/µl.

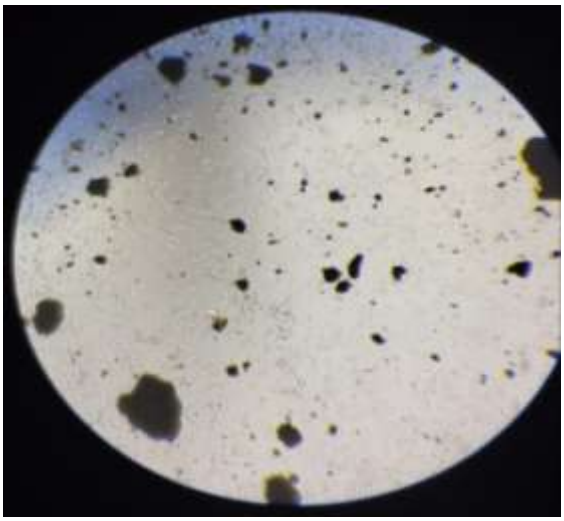

Figure 4.30 Treated U87 Glioblastoma cells against Ni-Co_3O_4 for 24 h, Magnification (10X)

Table 4.2 Nikel-doped Co_3O_4 Nanoparticles concentration and cell viability

Concentration (µg/µl)	Cell Viability %
100	**18.217**
200	**19.284**
300	**23.283**
400	**24.429**
500	**51.150**

Table 4.2 shows lower concentrations (100–300 µg/µL), cell viability remains low (18–23%), indicating strong cytotoxicity. As the concentration increases to 400 µl and 500

µl, viability rises to 24.43% and 51.15%, respectively. This suggests a non-linear response, where higher concentrations reduce toxicity, possibly due to nanoparticle aggregation or altered cellular interactions. Overall, the results highlight a dose-dependent but complex cytotoxic pattern.

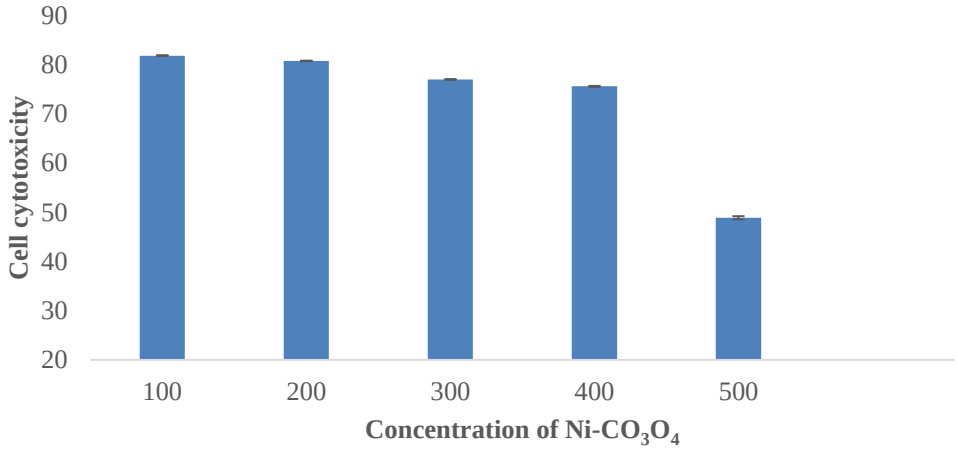

Figure 4.31 Cell cytotoxicity on U87 cell line by Ni-Co_3O_4 Nanoparticles (bars represent standard deviation of the mean).

Figure 4.31 shows the effect of Nickel-doped cobalt oxide nanoparticles on U87 brain cancer cell cytotoxicity.The cell cytotoxicity remains high (~78–81%) from 100 to 400 µg/µl, showing minimal variation. However, at 500 µg/µL, there is a sharp decrease in cytotoxicity to around 50%, indicating a potential toxic effect or reduced cell viability at higher concentration.

Ni–Co_3O_4 exhibits greater cytotoxicity at lower concentrations (100–200 µg/µL), whereas Zn–Co_3O_4 demonstrates superior effectiveness at higher concentrations (300–500 µg/µL), possibly resulting from size-related reactivity differences and variations in aggregation or ROS generation.

4. DISCUSSION

Nanotechnology encompasses the engineering of functional materials within the nanoscale range of 1–100 nm, presenting considerable promise in the fields of biomedicine and antimicrobial applications (Odemis, 2022). Pure Co_3O_4 exhibited very little biological activity, doping with Zn or Ni significantly improved antibacterial and anticancer efficacy.

In this investigation, pure Co_3O_4, Zn-doped Co_3O_4, and Ni-doped Co_3O_4 nanoparticles were synthesized utilizing the co-precipitation method and subsequently evaluated for their antibacterial and anticancer properties. The nanoparticles were analyzed through UV–Vis, FTIR, SEM, and XRD to determine their optical properties, morphology, and structural characteristics. For the assessment of antibacterial efficacy, the test organisms *Salmonella enteritidis, Acinetobacter sp., Klebsiella pneumoniae, and Staphylococcus aureus* were verified through Gram staining prior to analysis to ensure the precise identification of the strains and MacConkey agar for selective growth. It was observed that Ni-doped Co_3O_4 nanoparticles exhibited the highest antibacterial activity against *Klebsiella pneumoniae* and *Salmonella enteritidis*, while showing the weakest effect against *Acinetobacter* sp. In comparison, Zn doped Co_3O_4 nanoparticles displayed overall superior antibacterial performance, particularly against *Salmonella*, producing larger inhibition zones across most tested strains. Increased buildup of reactive oxygen species, metal ion release, and subsequent split of bacterial cell membranes may be the root of the doped nanoparticles' enhanced bactericidal activity (Ali *et al*., 2022).

The enhanced activity can be elucidated by the ability of nanoparticles to generate reactive oxygen species (ROS), inflict damage upon bacterial membranes, and liberate metal ions that obstruct microbial enzymatic functions. These results substantiate previous investigations that have illustrated the antibacterial potential of doped cobalt oxides (Ali *et al.,* 2022). Nickel-doped nanoparticles demonstrated a marginally more pronounced antibacterial efficacy in comparison to Zinc-doped nanoparticles, which may be attributed to their superior surface charge and catalytic properties (Patil *et al.,* 2021).

The MTT assay test was applied to evaluate the nanoparticles' anticancer impact on U87 glioblastoma cells. For Ni-Co_3O_4 nanoparticles, the observed cytotoxicity escalated from approximately 40% at a concentration of 100 µg/µL to roughly 65% at 300 µg/µL, followed by a decline at elevated concentrations, potentially attributable to nanoparticle aggregation and diminished cellular uptake. In contrast, Zn–Co_3O_4 nanoparticles exhibited a markedly steeper dose-dependent increase cytotoxicity was approximately 59% at 100 µg/µL, slightly elevated to 61% for 200 µg/µL, and attained nearly 99% at 300 µg/µL, ultimately surpassing 100% at concentrations ranging from 400 to 500 µg/µL. These findings substantiate that Zinc doping confers a more potent cytotoxic effect at elevated concentrations, whereas Nickel doping provides a more equitable yet marginally less pronounced cytotoxic profile. The mechanisms that underlie these phenomena are congruent with previous investigations indicating that Co_3O_4 based nanoparticles elicit anticancer effects through the induction of oxidative stress, mitochondrial damage, and the activation of apoptotic pathways (Huang *et al.,* 2021). Nickel-doped nanoparticles preserved higher activity at moderate concentrations, while Zinc-doped particles exhibited exceptional potency at high dosages, potentially due to their catalytic enhancement of reactive oxygen species (ROS) generation and redox interactions (Almoneef *et al.,* 2024).

Both Zinc and Nickel-doped Cobalt oxide (Co_3O_4) nanoparticles have been observed to enhance the biological activity of Cobalt oxide, albeit with distinct dose-response dynamics. The Nickel-doped nanoparticles exhibited sustained anticancer properties at intermediate concentrations, while the Zinc-doped counterparts induced a significant reduction in cell viability, with values descending into negative ranges at elevated doses. These discrepancies are likely attributable to the structural and electronic modifications resulting from the doping process, and the pronounced efficacy of both materials, even at comparatively low concentrations, underscores their potential for therapeutic applications as evidenced in the existing literature (Reena & Aslinjensipriya, 2023). The steep dose-response profiles of both nanoparticle types signify substantial biological efficacy, even at modest dosage levels, thereby emphasizing their prospective role as therapeutic agents.

In summary, Zinc-doped Cobalt oxide nanoparticles demonstrated the most significant biological activities, exhibiting the highest antibacterial inhibition against *Salmonella* and achieving complete cytotoxicity against U87 glioblastoma cells at a concentration of 500 µg/µL, thereby validating their enhanced therapeutic efficacy in comparison to both undoped and Nickel-doped Cobalt oxide counterparts.

REFERENCES

Al-Enazi, N. M., Alsamhary, K., Ameen, F., & Kha, M. (2023). Plant extract-mediated synthesis cobalt doping in Zinc oxide nanoparticles and their in vitro cytotoxicity and antibacterial performance. Heliyon, 9(9).

Akhtar, K., Khan, S. A., Khan, S. B., & Asiri, A. M. (2018). *Scanning electron microscopy: Principle and applications in nanomaterials characterization* (pp. 113-145). Springer International Publishing.

Alhalili, Z. (2023). Metal oxides nanoparticles: general structural description, chemical, physical, and biological synthesis methods, role in pesticides and heavy metal removal through wastewater treatment. *Molecules*, *28*(7), 3086.

Alhujaily, M., Albukhaty, S., Yusuf, M., Mohammed, M. K., Sulaiman, G. M., Al-Karagoly, H., ... & AlMalki, F. A. (2022). Recent advances in plant-mediated Zinc oxide nanoparticles with their significant biomedical properties. Bioengineering, 9(10), 541.

Ali, A., Chiang, Y. W., & Santos, R. M. (2022). X-ray diffraction techniques for mineral characterization: A review for engineers of the fundamentals, applications, and research directions. Minerals, 12(2), 205.

Ali, R., Patel, V., & Singh, P. (2022). Nickel-doped cobalt oxide nanostructures as potent antimicrobial agents against multidrug-resistant bacteria. Materials Science & Engineering C, 130(4), 112–119.

Almoneef, M. M., Awad, M. A., Aldosari, H. H., Hendi, A. A., Aldehish, H. A., Merghani, N. M., ... & Ahmed, M. S. (2024). Enhancing Biomedical and Photocatalytic Properties: Synthesis, Characterization, and Evaluation of Copper–Zinc Oxide Nanoparticles via Co-Precipitation Approach. Catalysts, 14(9), 641.

Anjum, S., Hashim, M., Malik, S. A., Khan, M., Lorenzo, J. M., Abbasi, B. H., & Hano, C. (2021). Recent advances in Zinc oxide nanoparticles (ZnO NPs) for cancer diagnosis, target drug delivery, and treatment. Cancers, 13(18), 4570.

Ansari, S. M., Younis, A., Kolekar, Y. D., & Ramana, C. V. (2025). Cobalt ferrite nanoparticles: The physics, synthesis, properties, and applications. Applied Physics Reviews, 12(2).

Arsalan, N., Hassan Kashi, E., Hasan, A., Edalat Doost, M., Rasti, B., Ahamad Paray, B., Zahed Nakhjiri, M., Sari, S., Sharifi, M., Shahpasand, K., Akhtari, K., Haghighat, S., & Falahati, M. (2020). Exploring the Interaction of Cobalt Oxide Nanoparticles with Albumin, Leukemia Cancer Cells and Pathogenic Bacteria by Multispectroscopic, Docking, Cellular and Antibacterial Approaches. International Journal of Nanomedicine, *15*, 4607–4623.

Bawoke. (2023, June 10 June 2023). Nanomaterials: An overview of synthesis, classification, characterization, and applications. willey, *4*(8), 486-501.

Bisht, G., & Rayamajhi, S. (2016). ZnO Nanoparticles: A Promising Anticancer Agent: *Nanobiomedicine, 3*, 9.

Bukhari, A., Ijaz, I., Gilani, E., Nazir, A., Zain, H., Saeed, R., ... & Naseer, Y. (2021). Green synthesis of metal and metal oxide nanoparticles using different plants' parts for antimicrobial activity and anticancer activity: a review article. Coatings, 11(11), 1374.

Correa, M. G., Martínez, F. B., Vidal, C. P., Streitt, C., Escrig, J., & de Dicastillo, C. L. (2020). Antimicrobial metal-based nanoparticles: A review on their synthesis, types and antimicrobial action. *Beilstein journal of nanotechnology*, *11*(1), 1450-1469.

Dakave, S. S., Bhinge, G. A., Shetti, S. S., & Kanamadi, C. M. (2023). Water treatment and electrocatalytic Oxygen Evolution Reaction of Cobalt Oxide nanoparticles.

Faisal, S., Jan, F. A., Saleem, S., Ullah, R., Wajidullah, Ullah, N., & Salman. (2022). J uglans regia L. mediated synthesis of cobalt oxide and Zinc-doped cobalt oxide nanoparticles: characterization and evaluation for environmental, antibacterial and cytotoxic potential. Nanotechnology for Environmental Engineering, 7(3), 675-689.

Farghal, F. E., & Abdel-Khalek, M. A. (2021). Exploitation of spent Nickel-metal hydride (Ni-MH) batteries as a source of value-added products. *Physicochemical Problems of Mineral Processing, 57*.

Farhat, S., Ouar, N., Hosni, M., Hinkov, I., Mercone, S., Schoenstein, F., & Jouini, N. (2014). Scale-Up of the Polyol Process for Nanomaterial Synthesis. *Journal of Materials Science and Chemical Engineering, 2014*.

Forsythe, R. C., Cox, C. P., Wilsey, M. K., & Muller, A. M. (2021). Pulsed laser in liquids made nanomaterials for catalysis. *Chemical Reviews, 121*(13), 7568-7637

Gorylewski, D., Zasada, F., Słowik, G., Lofek, M., Grzybek, G., Tyszczuk-Rotko, K., ... & Stelmachowski, P. (2025). Modulation of the Electronic Properties of Co3O4 through Bi Octahedral Doping for Enhanced Activity in the Oxygen Evolution Reaction. *ACS catalysis*, *15*(6), 4746-4758.

Govindasamy, R., Raja, V., Singh, S., Govindarasu, M., Sabura, S., Rekha, K., ... & Thiruvengadam, M. (2022). Green synthesis and characterization of cobalt oxide nanoparticles using Psidium guajava leaves extracts and their photocatalytic and biological activities. *Molecules*, *27*(17), 5646.

Geoprincy, G., Saravanan, P., Gandhi, N. N., & Renganathan, S. (2011). A novel approach for studying the combined antimicrobial effects of silver nanoparticles and antibiotics through agar over layer method and disk diffusion method. *Digest Journal of Nanomaterials and Biostructures*, *6*(4), 1557-1565.

Gutknecht, T., Colombus, Y., & Steenari, B. M. (2017). Recycling Zinc from metal oxide varistors through leaching and cementation of cobalt and Nickel. *Journal of Sustainable Metallurgy*, *3*, 239-250.

Huang, H., Wang, J., Zhang, J., Cai, J., Pi, J., & Xu, J. F. (2021). Inspirations of cobalt oxide nanoparticle based anticancer therapeutics. *Pharmaceutics*, *13*(10), 1599.

Iqbal, A., Khan, T. F., & Iqbal, Y. (2024). Nanobiotechnology. In *Handbook of Nanomaterials, Volume 2* (pp. 685-713). Elsevier.

Iqbal, J., Abbasi, B. A., Mahmood, T., Kanwal, S., Ali, B., & Khalil, A. T. (2021). Antibacterial and cytotoxic potential of cobalt oxide nanoparticles: synthesis via green route using *Salvia officinalis* extract. *Materials Research Express*, 8(3), 035005.

Jana, M., Sil, A., & Ray, S. (2016). Chemical nature of catalysts of oxide nanoparticles in the environment prevailing during growth of carbon nanostructures by ccvd. Bulletin of Materials Science, 39(7), 1783-1790

Jarestan, M., Khalatbari, K., Pouraei, A., Sadat Shandiz, S. A., Beigi, S., Hedayati, M., Majlesi, A., Akbari, F., & Salehzadeh, A. (2020). Preparation, characterization, and anticancer efficacy of novel cobalt oxide nanoparticles conjugated with thiosemicarbazide. 3 Biotech, *10*(5), 230.

Jarvie, H., Dobson, P., King, S. (2024, August 31). nanoparticle. Encyclopedia Britannica. https://www.britannica.com/science/nanoparticle

Jiang, J., Pi, J., & Cai, J. (2018). The advancing of Zinc oxide nanoparticles for biomedical applications. *Bioinorganic chemistry and applications*, *2018*(1), 1062562.

Kalpana, S., Krishnan, S. S., Senthil, T. S., & Elangovan, S. V. (2017). Cobalt doped Zinc oxide nanoparticles for photocatalytic applications. *J. Ovonic Res*, *13*, 263-269.

Khalid, A., Ahmad, P., Alharthi, A. I., Muhammad, S., Khandaker, M. U., Faruque, M. R. I., ... & Bradley, D. A. (2021). Enhanced optical and antibacterial activity of hydrothermally synthesized cobalt-doped Zinc oxide cylindrical microcrystals. Materials, 14(12), 3223.

Khalil, A. T., Ovais, M., Ullah, I., Ali, M., Shinwari, Z. K., Hassan, D., & Maaza, M. (2018). Sageretia thea (Osbeck.) modulated biosynthesis of NiO nanoparticles and their in vitro pharmacognostic, antioxidant and cytotoxic potential. Artificial cells, nanomedicine, and biotechnology, 46(4), 838-852.

Khan, M., Ali, S., & Ahmad, N. (2023). Enhanced antibacterial activity of Zinc-doped cobalt oxide nanoparticles: Mechanistic insights. Journal of Nanobiotechnology, 21(5), 123–135.

Krishnamoorthy, R., Athinarayanan, J., Periyasamy, V., Alshuniaber, M. A., Al-Shammari, G. M., Hakeem, M. J., Ahmed, M. A., & Alshatwi, A. (2022). Antibacterial mechanisms of Zinc oxide nanoparticles against bacterial food pathogens resistant to beta-lactam antibiotics. Molecules. https://doi.org/10.3390/molecules27082489

Kulandaivel, A. and Hemalatha, J. (2022). Extensive analysis on the thermoelectric properties of aqueous zn-doped Nickel ferrite nanofluids for magnetically tuned thermoelectric applications. ACS Applied Materials &Amp; Interfaces, 14(23), 26833-26845. https://doi.org/10.1021/acsami.2c06457

Kumari, S., Raturi, S., Kulshrestha, S., Chauhan, K., Dhingra, S., András, K., ... & Singh, T. (2023). A comprehensive review on various techniques used for synthesizing nanoparticles. Journal of Materials Research and Technology, 27, 1739-1763.

Mahmood, F., Zehra, S. S., Hasan, M., Zafar, A., Tariq, T., Abdullah, M., ... & Shu, X. (2023). Bioinspired cobalt oxide nanoball synthesis, characterization, and their potential as metal stress absorbants. *ACS omega*, *8*(6), 5836-5849.

Mejía, C., Hoeven, J., Jongh, P., & Jong, K. (2020). Cobalt–Nickel nanoparticles supported on reducible oxides as fischer–tropsch catalysts. Acs Catalysis, 10(13), 7343-7354. https://doi.org/10.1021/acscatal.0c00777

Mekuye, B., & Abera, B. (2023). Nanomaterials: An overview of synthesis, classification, characterization, and applications. Nano Select. https://doi.org/10.1002/nano.202300038

Moradpoor, H., Safaei, M., Rezaei, F., Golshah, A., Jamshidy, L., Hatam, R., & Abdullah, R. S. (2019). Optimisation of cobalt oxide nanoparticles synthesis as bactericidal agents. *Open access Macedonian journal of medical sciences*, *7*(17), 2757.

Mayakannan, M., Gopinath, S., & Vetrivel, S. (2020). Synthesis and characterization of antibacterial activities Nickel-doped cobalt oxide nano particles. *Materials Chemistry and Physics*, *242*, 122282.

Mayakannan, M., Prabakar, S., & Vinoth, E. (2023). Synthesis and characterizations of Zinc-doped cobalt oxide nanoparticles and its antibacterial and antifungal activities. *Inorganic and Nano-Metal Chemistry*, *53*(12), 1329-1335

Naik, T. A., & Mallikarjun, N. Optimization of Mycosynthesis of Silver Nanoparticles from Aspergillus flavus.

Naseri, M., Dehzangi, A., Kamari, H. M., See, A., Abedi, M., Salasi, R., ... & Majlis, B. Y. (2016). Structure and physical properties of NiO/Co3O4 nanoparticles. Metals, 6(8), 181.

Nawaz, M., & Kaus, N. (2020). Environmental and agricultural applications of cobalt oxide nanoparticles. *Environmental Nanotechnology*, 7(2), 112–120.

Nawaz, M., Anwar, S., Haider, S., & Nasir, M. (2023). Synergistic antimicrobial potential of Zn and Ni co-doped cobalt oxide nanoparticles synthesized by sol–gel method. *Journal of Materials Science: Materials in Medicine*, 34(1), 12.

Niakan, S., Niakan, M., Hesaraki, S., Nejadmoghaddam, M. R., Moradi, M., Hanafiabdar, M., ... & Sabouri, M. (2013). Comparison of the antibacterial effects of nanosilver with

18 antibiotics on multidrug resistance clinical isolates of Acinetobacter baumannii. *Jundishapur Journal of Microbiology*, *6*(5), 1Q.

Odero, J., Lilechi, M. C., & Nyanchoga, S. (2024). Synthesis and characterization of cobalt-doped zno nanoparticles with enhanced photocatalytic activity. Journal of Educational Research and Policies. https://doi.org/10.53469/jerp.2024.06(08).10

Oves, M., Arshad, M. K. M., Khan, M. S., Ahmed, A. S., Azam, A., & Ismail, I. M. (2015). Antimicrobial activity of cobalt doped Zinc oxide nanoparticles: targeting water borne bacteria. Elsevier BV. https://doi.org/10.1016/j.jscs.2015.05.003

Patel, R., & Patel, C. (2014). *Quantitative Analytical applications of FTIR Spectroscopy in Pharmaceutical and Allied Areas*.

Patil, S., Desai, K., & Sharma, R. (2021). Synthesis and characterization of Zn/Ni-Co_3O_4 nanoparticles for biomedical applications: A review on antibacterial mechanisms. Nanomedicine Research Journal, 10(3), 45–57.

Potes-Lesoinne, H., Ramirez-Alvarez, F., Pérez-González, V., Martínez-Chapa, S., & Gallo-Villanueva, R. (2021). Nanomaterials for electrochemical detection of pollutants in water: a review. Electrophoresis, 43(1-2), 249-262.

Reena, R. S., Aslinjensipriya, A., Infantiya, S. G., Britto, J. D. J., Jose, M., & Das, S. J. (2022). Visible-light active Zinc-doped cobalt oxide (Zn-Co3O4) nanoparticles for photocatalytic and photochemical activity. *Materials Today: Proceedings*, *68*, 269-275.

Rami, J. M., & Patel, C. D. (2023). Exploration of significant optical parameters of selected metal oxide nanoparticles using optical spectroscopy. NanoWorld J., 9(S1), S601-S605.

Rana, A. G. (2022). *Modification of Graphitic Carbon Nitride (gC 3 N 4) for photocatalytic redox reactions* (Doctoral dissertation, Technische Universität München).

Rana, S. B., & Singh, R. P. (2016). Investigation of structural, optical, magnetic properties and antibacterial activity of Ni-doped Zinc oxide nanoparticles. *Journal of Materials Science: Materials in Electronics*, *27*(9), 9346-9355.

Saeed, S. Y., Mazhar, K., Raees, L., Mukhtiar, A., Khan, F., & Khan, M. (2022). Green synthesis of cobalt oxide nanoparticles using roots extract of Ziziphus Oxyphylla

Edgew its characterization and antibacterial activity. *Materials Research Express*, *9*(10), 105001.

Salah, N., Habib, S. S., Khan, Z. H., Memic, A., Azam, A., Alarfaj, E., ... & Al-Hamedi, S. (2011). High-energy ball milling technique for ZnO nanoparticles as antibacterial material. *International journal of nanomedicine*, 863-869.

sanjay singh. (2023). Nanoparticles: Their Classification, Types and Properties. IJIRT, *9*(8), 157866. https://ijirt.org/publishedpaper/IJIRT157866_PAPER.pdf

Schiopu, A. G., Iordache, D. M., Oproescu, M., Cursaru, L. M., & Ioța, A. M. (2024). Tailoring the synthesis method of metal oxide nanoparticles for desired properties. Crystals, 14(10), 899.

Shahcheraghi, N., Golchin, H., Sadri, Z., Tabari, Y., Borhanifar, F., & Makani, S. (2022). Nano-biotechnology, an applicable approach for sustainable future. 3 Biotech, 12(3), 65.

Shenoy, R. U. K., Rama, A., Govindan, I., & Naha, A. (2022). The purview of doped nanoparticles: Insights into their biomedical applications. OpenNano, 11, 100070.

Shete, R. C., Fernandes, P. R., Borhade, B. R., Pawar, A. A., Sonawane, M. C., & Warude, N. S. (2022). Review of cobalt oxide nanoparticles: Green synthesis, biomedical applications, and toxicity studies. J. Chem. Rev, 4, 331-345.

Sirelkhatim, A., Mahmud, S., Seeni, A., Kaus, N. H. M., Ann, L. C., Bakhori, S. K. M., Hasan, H., & Mohamad, D. (2015). Review on Zinc oxide nanoparticles: antibacterial activity and toxicity mechanism. *Nano-Micro Letters*, 7(3), 219–242.

Srinisha, M., Jeevitha, M., Rajeshkumar, S., & Jayaraman, S. (2021). Cytotoxic activity of Zinc oxide nanoparticle synthesis using leaves extract of Abies webbiana. *J Pharm Rest Int*, *33*, 3716-23.

Sune, P. R., Jumde, K. S., Hatwar, P. R., Bakal, R. L., More, S. D., & Korde, A. V. (2024). Nanoparticles: Classification, types and applications: A comprehensive review.

Ullah, I., Neder, R. B., Ahmad, M., Khan, A. Q., Rauf, A., Alshammari, A., & Albekairi, N. A. (2024). Antimicrobial activities and neuroprotective potential for Alzheimer's disease of pure, Mn, Co, and Al-doped ZnO ultra-small nanoparticles. *Green Processing and Synthesis*, *13*(1), 20240096.

Vinardell, M. P., & Mitjans, M. (2015). Antitumor activities of metal oxide nanoparticles. *Nanomaterials*, *5*(2), 1004-1021.

Vinosha, P. A., Manikandan, A., Ceicilia, A. S. J., Dinesh, A., Nirmala, G. F., Preetha, A. C., ... & Xavier, B. (2021). Review on recent advances of Zinc substituted cobalt ferrite nanoparticles: Synthesis characterization and diverse applications. *Ceramics International*, *47*(8), 10512-10535.

Wang, J. W., & Kuo, Y. M. (2013). Synthesis of Nanosized Zinc-Doped Cobalt Oxyhydroxide Parties by a Dropping Method and Their Carbon Monoxide Gas Sensing Properties. *Journal of Nanomaterials*, *2013*(1), 136145.

Waris, A., Din, M., Ali, A., Afridi, S., Baset, A., Khan, A. U., & Ali, M. (2021). Green fabrication of Co and Co3O4 nanoparticles and their biomedical applications: A review. Open life sciences, 16(1), 14-30.

Xu, Y., & Zhang, L. (2018). Surface modification of nanoparticles for targeted drug delivery. *Nanotechnology Reviews*, 7(4), 223–235.

Yin, H., Lu, Y., Chen, R., Orrell-Trigg, R., Gangadoo, S., Chapman, J., ... & Truong, V. K. (2024). Cytotoxicity and Antimicrobial Efficacy of Fe-, Co-, and Mn-Doped ZnO Nanoparticles. *Molecules*, *29*(24), 5966

Zakharova, O., Kolesnikov, E., Vishnyakova, E., Strekalova, N., & Gusev, A. (2019, February). Antibacterial activity of ZnO nanoparticles: dependence on particle size, dispersion media and storage time. In *IOP Conference Series: Earth and Environmental Science* (Vol. 226, p. 012062). IOP Publishing.

Zhang, Z., Li, L., Xu, Q., & Cao, B. (2015). 3D hierarchical Co 3 O 4 microspheres with enhanced lithium-ion battery performance. *RSC Advances*, *5*(76), 61631-61638.